HHS Public Access

Author manuscript

Nat Med. Author manuscript; available in PMC 2019 July 21.

Small-molecule targeting of brachyury transcription factor addiction in chordoma

Tanaz Sharifnia[1,20,*], **Mathias J. Wawer**[1], **Ting Chen**[2], **Qing-Yuan Huang**[2,11], **Barbara A. Weir**[1,12], **Ann Sizemore**[1,13], **Matthew A. Lawlor**[3,14], **Amy Goodale**[1], **Glenn S. Cowley**[1,15], **Francisca Vazquez**[1], **Christopher J. Ott**[3,14], **Joshua M. Francis**[1,16], **Slim Sassi**[4,5], **Patricia Cogswell**[6], **Hadley E. Sheppard**[7], **Tinghu Zhang**[3], **Nathanael S. Gray**[3], **Paul A. Clarke**[8], **Julian Blagg**[8], **Paul Workman**[8], **Josh Sommer**[6], **Francis Hornicek**[4,17], **David E. Root**[1], **William C. Hahn**[1,3], **James E. Bradner**[3,18], **Kwok K. Wong**[2], **Paul A. Clemons**[1], **Charles Y. Lin**[7,20,*], **Joanne D. Kotz**[1,19,20,*], and **Stuart L. Schreiber**[1,9,10,20,*]

[1]Broad Institute of Harvard and MIT, Cambridge, MA 02142, USA

[2]New York University Langone Medical Center, New York, NY 10016, USA

[3]Dana-Farber Cancer Institute, Boston, MA 02215, USA

[4]Massachusetts General Hospital, Boston, MA 02114, USA

---

*Correspondence: tanaz@broadinstitute.org (T.S.), Charles.Y.Lin@bcm.edu (C.Y.L.), jkotz@jnanatx.com (J.D.K.), and stuart_schreiber@harvard.edu (S.L.S.).

[5]Harvard Medical School, Boston, MA 02115, USA

[6]Chordoma Foundation, Durham, NC 27702, USA

[7]Baylor College of Medicine, Houston, TX 77030, USA

[8]Cancer Research UK Cancer Therapeutics Unit, The Institute of Cancer Research, London SW7 3RP, United Kingdom

[9]Harvard University, Cambridge, MA 02138, USA

[10]Howard Hughes Medical Institute, Chevy Chase, MD 20815, USA

[11]Present address: Shanghai General Hospital, Shanghai Jiao Tong University, Shanghai 200000, China

[12]Present address: Janssen R&D, Cambridge, MA 02142, USA

[13]Present address: University of Pennsylvania, Philadelphia, PA 19104, USA

[14]Present address: Massachusetts General Hospital, Charlestown, MA 02129, USA

[15]Present address: Janssen R&D, Spring House, PA 19477, USA

[16]Present address: Gritstone Oncology, Cambridge, MA 02142, USA

[17]Present address: UCLA Medical Center, Santa Monica, CA 90404, USA

[18]Present address: Novartis Institutes for BioMedical Research, Cambridge, MA 02139, USA

[19]Present address: Jnana Therapeutics, Boston, MA 02210, USA

[20]These authors jointly supervised this work: Tanaz Sharifnia, Charles Y. Lin, Joanne D. Kotz, Stuart L. Schreiber

Chordoma is a primary bone cancer with no approved therapy[1]. The identification of therapeutic targets in this disease has been challenging due to the infrequent occurrence of clinically actionable somatic mutations in chordoma tumors[2,3]. Here we describe the discovery of therapeutically targetable chordoma dependencies via genome-scale CRISPR-Cas9 screening and focused small-molecule sensitivity profiling. These systematic approaches reveal that the developmental transcription factor T (brachyury; *TBXT*) is the top selectively essential gene in chordoma, and that transcriptional cyclin-dependent kinase (CDK) inhibitors targeting CDK7/12/13 and CDK9 potently suppress chordoma cell proliferation. In other cancer types, transcriptional CDK inhibitors have been observed to downregulate highly expressed, enhancer-associated oncogenic transcription factors (TFs)[4,5]. In chordoma, we find that T is associated with a 1.5-Mb region containing "super-enhancers" and is the most highly expressed super-enhancer-associated TF. Notably, transcriptional CDK inhibition leads to preferential and concentration-dependent downregulation of cellular brachyury protein levels in all models tested. *In vivo*, CDK7/12/13-inhibitor treatment substantially reduces tumor growth. Together, these data demonstrate small-molecule targeting of brachyury TF addiction in chordoma, identify a mechanism of T gene regulation that underlies this therapeutic strategy, and provide a

blueprint for applying systematic genetic and chemical screening approaches to discover vulnerabilities in genomically quiet cancers.

Chordoma is a primary bone cancer that typically occurs in the skull-base, mobile spine, and sacrum[6]. Chordoma often manifests as a slow-growing but locally invasive malignancy, with a tendency to recur despite surgical and/or radiation therapy[1,7]. There are no approved targeted therapies, conventional cytotoxic chemotherapies, or immunotherapies for chordoma[1]. The lack of systemic treatment options, and an inadequate understanding of chordoma biology to guide the development of new therapies, contributes to poor prognoses for patients with advanced disease[7].

Chordoma is hypothesized to originate from embryonic notochordal remnants[8]. Both cell types share high expression of the T-box-family TF brachyury (gene symbol: *T*; *TBXT*)[9], an essential regulator of notochord development[10] whose overexpression is characteristic of chordoma[9]. Beyond being a chordoma biomarker, brachyury appears to be critical for disease pathogenesis: germline *T* duplication confers susceptibility to familial chordoma[11], a single-nucleotide polymorphism (SNP) in *T* is associated with chordoma[12], some sporadic chordomas harbor somatic copy-number gains of *T*[3,13], and *T* silencing inhibits growth of chordoma models[13–15]. Furthermore, brachyury is primarily expressed in the embryo and is absent from the majority of normal adult tissue[9,10,16]. These findings suggest that brachyury may act as an aberrantly activated developmental TF that is oncogenic and essential in a lineage-specific manner, akin to canonical "lineage-survival" oncogenes (e.g., *MITF* in melanoma)[17].

Importantly, however, the full range of tumor dependencies in chordoma is not known. Few genes are recurrently mutated—and only at a modest frequency—in sporadic chordomas[2,3]; and nearly half of sporadic cases have no known driver mutation[3]. Furthermore, no systematic functional genomics studies have been conducted in chordoma models. Thus, it remains unclear if brachyury represents the central tumor dependency of chordoma, or whether there are critical dependencies left to be uncovered, and, if the former, whether brachyury overexpression can be targeted therapeutically. Like other TFs, brachyury is not readily inhibited pharmacologically[18], and no small-molecule inhibitor of brachyury has been identified. It is also not known what underlies brachyury dysregulation in the majority of chordoma tumors, and whether any potential mediators of overexpression are therapeutically targetable. Somatic alterations in *T* occur in a minority of sporadic chordomas[3] and cannot explain the nearly universal occurrence of brachyury expression. Therefore, a deeper understanding of essential genes in chordoma, including potential regulators of brachyury expression, is imperative for nominating candidate therapeutic targets.

Recent advances in systematic CRISPR-Cas9 screening and small-molecule sensitivity profiling approaches have enabled identification of tumor dependencies in multiple cancer types[19]. We integrated these complementary approaches to identify key tumor dependencies and candidate therapeutic targets in chordoma.

T is a selectively essential gene in chordoma

To identify genes essential for chordoma cell viability, we performed genome-scale pooled CRISPR-Cas9 loss-of-function screens in two chordoma cell lines (UM-Chor1, MUG-Chor1). We introduced a library of >74,000 single-guide RNAs (sgRNAs) targeting ~18,560 genes (Methods) into stably Cas9-expressing cells via lentiviral transduction, and after 21 days, quantified sgRNAs from the genomic DNA of surviving cells. Depleted sgRNAs, representing candidate essential genes, were identified by comparing these sgRNA abundances to those of the screening library. We ranked all sgRNAs by how much they reduced viability in chordoma cells relative to 125 non-chordoma cancer cell lines screened using the same sgRNA library (Broad Institute Project Achilles; https://depmap.org/portal/achilles/)[20], thus removing commonly essential genes to identify dependencies selective for chordoma.

The top three selectively lethal sgRNAs, out of ~70,000 sgRNAs analyzed, all targeted the *T* gene (Fig. 1a). We confirmed that three of four *T*-targeted sgRNAs screened were lethal to both chordoma cell lines, but not to 125 non-chordoma cancer cell lines (Fig. 1b and Supplementary Table 1). Targeting *T* in chordoma cells induced a similar degree of viability reduction as targeting commonly essential ribosomal subunit genes *RPL23*, *RPS11*, and *RPS19* (Fig. 1b, Extended Data Fig. 1, and Supplementary Table 1), indicating that chordoma cells are both exquisitely and selectively sensitive to loss of brachyury expression.

We validated the screening results with two sgRNAs targeting independent sequences of *T* in three chordoma cell lines (UM-Chor1, MUG-Chor1, U-CH2) (Fig. 1c). The observed reduction in chordoma cell proliferation induced by sgRNA-mediated brachyury repression was consistent with previously reported effects of shRNA-mediated gene silencing of *T* in other chordoma cell lines[13,14].

SgRNA-mediated *T* repression in UM-Chor1 cells led to downregulation of canonical notochord markers (*SOX9*, *COL2A1*, *ACAN*) (Fig. 1d), consistent with brachyury's known role in notochord development[21]. Additionally, genes associated with the G2/M checkpoint and E2F targets were enriched among downregulated genes (Fig. 1e), suggestive of cell cycle arrest in sg-*T*-expressing cells. These data implicate *T* as an essential gene and regulator of notochord cell identity in chordoma.

Inhibitors of CDK7/12/13 and CDK9 suppress chordoma cell proliferation

In parallel to the genetic screens, we tested 459 small molecules for their ability to reduce proliferation or survival in four chordoma cell lines. Compounds were selected to collectively target many distinct nodes in cell circuitry, and included FDA-approved drugs, preclinical agents, and small-molecule probes (Supplementary Table 2). A largely overlapping small-molecule library was previously tested in ~800 non-chordoma cancer cell lines[22], and we used these data to identify and prioritize compounds with antiproliferative effects selective for chordoma when possible (Fig. 2a; Methods).

Our analysis identified 28 potent antiproliferative compounds, including several inhibitors of either CDK7,12,13; CDK9; or EGFR/ERBB2 proteins (Fig. 2a and Supplementary Table 2).

As CDK7 and CDK9 have related roles in regulating transcription[23], we hypothesized that these inhibitor classes could have similar mechanistic effects.

The sensitivity of chordoma cells to compounds targeting CDK7/12/13 (THZ1)[4]; CDK12/13 (THZ531)[24]; CDK9 (NVP-2, AT7519, dinaciclib, alvocidib)[23,25]; and EGFR and/or ERBB2 (erlotinib, neratinib, canertinib, lapatinib, afatinib)[26] was validated using multipoint concentration-response assays (Fig. 2b, Extended Data Fig. 2a, and Supplementary Table 3). Transcriptional CDK inhibitors including THZ1, dinaciclib, and alvocidib exhibit antiproliferative effects across a diversity of cancer cell lines[4] (Extended Data Fig. 2b). Consistent with small-molecule sensitivity findings, sgRNAs targeting CDK7, CDK13, and CDK9, but not those targeting CDK12, were lethal to chordoma cells (Fig. 2c and Supplementary Table 1). SgRNAs targeting EGFR and ERBB2 were lethal to 2/2 and 1/2 chordoma cell lines, respectively (Fig. 2c and Supplementary Table 1). EGFR-inhibitor sensitivity in chordoma has been described previously[27]; thus, we focused on transcriptional CDK inhibitors, which are newly identified antiproliferative agents in chordoma.

We confirmed on-target activity of the CDK7/12/13 inhibitor THZ1 by detecting reduced phosphorylation, particularly at serine 2, of the C-terminal domain (CTD) of RNA polymerase II (POLR2A) (Fig. 2d). Beyond having antiproliferative effects, THZ1 treatment induced apoptosis in chordoma cells, as measured by increased caspase-3/7 activity (Fig. 2e). We did not observe comparable sensitivity of chordoma cells to inhibitors of CDK proteins not implicated in direct phosphorylation of the POLR2A CTD, including CDK4/6 inhibitors (palbociclib/PD 0332991, LEE011)[28]; and CDK8/19 inhibitors (CCT251545, BRD6989)[29,30] (Extended Data Fig. 3a and Supplementary Table 3). On-target activity was confirmed for a select number of CDK inhibitors tested (Extended Data Fig. 3b). Together, these data implicate inhibitors of CDK7/12/13 and CDK9 as potent antiproliferative agents in chordoma.

T is super-enhancer-associated in chordoma

Transcriptional CDK inhibitors are under clinical investigation (NCT03134638) owing to their ability to downregulate preferentially oncogenic TFs in multiple cancer types[5]. Components of the transcriptional apparatus, including CDK7, can densely occupy super-enhancers—large clustered enhancers that drive genes required for tumor identity—often rendering the expression of super-enhancer-driven genes especially vulnerable to transcriptional inhibitors[4,5,31,32]. To investigate whether similar mechanisms connect the essentiality of *T* to the antiproliferative effects of transcriptional CDK inhibitors, we tested whether *T* is super-enhancer-associated in chordoma.

We mapped the enhancer landscape in five chordoma cell lines using chromatin immunoprecipitation sequencing (ChIP-seq) to detect histone H3 lysine 27 acetylation (H3K27ac), a chromatin modification associated with active enhancers[32]. We identified large enhancers overlapping and adjacent to the *T* locus in all five models (Fig. 3a, Extended Data Fig. 4, and Supplementary Table 4). *T* enhancers showed evidence of brachyury binding, as measured by brachyury ChIP-seq (using a published dataset[33]) (Fig. 3a), and potentially other TFs as suggested by an assay for transposase-accessible chromatin using

sequencing (ATAC-seq) (Fig. 3a), which measures chromatin accessibility and TF occupancy[34]. In contrast, super-enhancers and brachyury binding were not detected at the housekeeping TF *MAX* locus, despite the presence of other TF binding sites as inferred by ATAC-seq signal (Fig 3b and Supplementary Table 4).

All chordoma cell lines had high *T* (brachyury) expression, especially compared to non-super-enhancer-associated genes, such as *MAX* (Fig. 3b–c and Extended Data Fig. 5a); in contrast, *T* (brachyury) was not widely expressed in non-chordoma cancer cell lines (Extended Data Fig. 5a–b). Furthermore, *T* expression was highest among all super-enhancer-associated TFs in chordoma (Fig. 3d and Extended Data Fig. 5c), and when ranked against all other enhancers, the *T*-associated super-enhancer was among the largest in the chordoma genome (Fig 3e, Supplementary Table 5, and Extended Data Fig. 4). JHC7 cells had a large focal amplification at the *T* locus that encompassed adjacent *T* enhancers, as well as a 1.5-Mb upstream region with broad H3K27ac occupancy (Fig. 3f and Extended Data Fig. 5d).

T-associated super-enhancers were similarly observed in patient-derived chordoma tumors (Supplementary Table 6), as detected by enhancer rank averaged across eight tumors (Fig. 3g and Supplementary Table 7) and in individual tumors (Fig. 3h, Extended Data Fig. 6, and Supplementary Table 4). Brachyury expression was confirmed for the subset of tumors tested (Extended Data Fig. 7). By enhancer ranking (Extended Data Fig. 6), 4/8 tumors had *T*-adjacent super-enhancers, 7/8 had *T*-adjacent enhancers ranking in the top 10% of all enhancers, and 8/8 were hyper-acetylated in the 1.5-Mb region found in JHC7 cells (Fig. 3i). In contrast, matched normal adjacent tissue lacked H3K27ac occupancy within this 1.5-Mb tumor hyper-acetylated region (Fig. 3i).

Enhancer patterns across tumors and cell lines showed grouping by *in vivo* or *ex vivo* state (Fig. 3j), similar to other cancer types[35]. Nonetheless, in both tumors and cell lines, super-enhancers associated with genes known to be highly expressed in chordoma: components of the extracellular matrix or its interactors (e.g., integrin subunit alpha 3, tensin 3, fibronectin 1, caveolin 1/2), mediators of de-differentiation (HoxA), and EGFR[36–38]. Thus, as in other cancers, super-enhancers associate with genes that define chordoma identity[31,32], and regulation of *T* by super-enhancers is a dominant feature of the chordoma gene-regulatory landscape.

Transcriptional CDK inhibition downregulates *T* (brachyury) expression preferentially

The essentiality of *T*, together with its association with super-enhancers, led us to test whether the antiproliferative effects of transcriptional CDK inhibitors are mediated by preferential loss of brachyury expression.

We found that THZ1 treatment reduced cellular brachyury protein levels in MUG-Chor1 and UM-Chor1 cells in a concentration- and time-dependent manner (Fig 4a and Extended Data Figure 8a). In contrast, brachyury protein expression was unchanged following treatment with compounds that are cytotoxic to chordoma cells but are not transcriptional CDK

inhibitors (Supplementary Table 2), including inhibitors of EGFR (erlotinib), Src (dasatinib), and the BET bromodomain (JQ1) (Fig. 4a). Downregulation of brachyury expression was also observed following treatment with CDK9 inhibitors (NVP-2, dinaciclib, alvocidib), but not with the CDK4/6 inhibitor palbociclib, across multiple chordoma models (Fig. 4b).

THZ1 treatment also substantially reduced mRNA expression of *T*, especially compared to *MAX* or the housekeeping gene *CFL1* (Extended Data Fig. 8b). For comparison, we tested actinomycin D, a transcriptional inhibitor not thought to act through CDK inhibition[39], and similarly observed mRNA downregulation of *T*, but not *MAX* or *CFL1* (Extended Data Fig. 8b). However, compared to THZ1, actinomycin D induced higher cytotoxicity at concentrations leading to substantial *T*-mRNA downregulation (Extended Data Fig. 8b–c and Supplementary Table 3), suggesting that THZ1 and actinomycin D could differ in how selectively they induce *T* downregulation.

We confirmed this difference using transcriptome-wide gene-expression profiling of THZ1- and actinomycin D-treated cells (Fig. 4c). Only THZ1 treatment led to preferential downregulation of *T* expression (Fig. 4c), indicating that super-enhancer-driven *T* transcription is particularly vulnerable to CDK7/12/13 inhibition.

Furthermore, we tested whether THZ1's antiproliferative effects are mediated by loss of super-enhancer-driven brachyury expression. To dissociate *T* from its endogenous regulatory elements, we transduced UM-Chor1 cells with an ORF encoding *T* under the control of an exogenous promoter. Unlike endogenous brachyury protein, ectopic brachyury expression levels were not greatly reduced with THZ1 treatment (Fig. 4d). Moreover, ectopic brachyury expression was sufficient to partially rescue loss of viability induced by 500 nM THZ1 treatment (Fig. 4e). Thus, downregulation of brachyury via its endogenous regulatory elements directly contributes to the antiproliferative effects of THZ1.

Besides *T*, only four genes were identified to be both super-enhancer-associated and essential in UM-Chor1 and MUG-Chor1 cells: *SOX9*, *SAE1*, *TPX2*, and *ATP6V1B2* (Fig. 4f). These genes appear to be under direct and/or indirect transcriptional control by brachyury: sgRNA-mediated *T* repression significantly reduced expression levels of all four genes (Fig. 4f, Supplementary Table 8, and Extended Data Fig. 9); and brachyury bound genomic regions corresponding to two of them (*SAE1* and *ATP6V1B2*; Fig. 4f and Supplementary Table 8).

These data support a model whereby *T* (brachyury) is expressed at high levels by a super-enhancer, is auto-regulated, and through direct binding to other super-enhancers and/or indirect mechanisms, can regulate other essential, super-enhancer-associated genes (Fig. 4g). As transcriptional CDKs including CDK7 and CDK9 are localized at enhancers[4,31], these data implicate transcriptional CDK inhibition in both upstream and downstream targeting of *T* (brachyury) gene control.

Finally, THZ1 efficacy was tested *in vivo*. A xenograft mouse model was generated with the human chordoma cell line CH22[40]. *Ex vivo*, CH22 cells were sensitive to transcriptional CDK inhibitors (Extended Data Fig. 10a), and compound treatment induced downregulation of brachyury expression (Extended Data Fig. 10b). Mice were treated with 40 mg/kg THZ1

BID, on a pulse-dosing schedule (Fig. 4h). This dose was reasonably well tolerated (Extended Data Fig. 10c), and was empirically determined to downregulate brachyury expression in target engagement studies of mouse tumors (Extended Data Fig. 10d), although we note that detection of brachyury downregulation varied across experiments and mice (Extended Data Fig. 10e).

THZ1 treatment led to a significant tumor-suppressive effect (p = 1.1×10^{-5}; Fig. 4i and Supplementary Table 9). These data provide evidence for the *in vivo* efficacy of THZ1 for the treatment of chordoma.

In conclusion, these findings nominate transcriptional CDK inhibition as a therapeutic strategy to target brachyury-driven transcriptional addiction in chordoma. Our results indicate that *T* (brachyury), a transcriptional regulator of notochord development, might drive chordoma tumorigenesis when dysregulated or persistently expressed. Thus, *T* resembles other "lineage-survival" oncogenes (e.g., *MITF* in melanoma), which arise from dysregulated expression of master genes that mediate normal lineage development[17]. More generally, these findings provide evidence for "transcriptional addiction" in chordoma, a state of exquisite dependence on specific regulators of gene expression[5]. As transcriptional dependencies are not typically discovered by tumor genome sequencing, these findings underscore the value of functional screening approaches, such as CRISPR-Cas9 and small-molecule sensitivity screening, to identify key vulnerabilities that may not manifest as mutations in the tumor genome.

TFs including brachyury are challenging to target directly with candidate drugs. Transcriptional CDK inhibition provides a therapeutic opportunity to downregulate preferentially *T* (brachyury). The recent entrance of next-generation transcriptional CDK inhibitors into the clinic may provide a much-needed therapeutic option for chordoma patients with refractory disease.

METHODS

Cell lines

UM-Chor1, MUG-Chor1, U-CH1, U-CH2, and JHC7 chordoma cell lines were obtained from the Chordoma Foundation. CH22 cells were obtained from the Chordoma Foundation and Massachusetts General Hospital and have been described previously[40]. UM-Chor1 cells were maintained in IMDM/RPMI (4:1) media + 10% fetal bovine serum (FBS) and 1X non-essential amino acids. MUG-Chor1, U-CH1, and U-CH2 cell lines were maintained in IMDM/RPMI (4:1) media + 10% FBS. JHC7 cells were maintained in DMEM/F12 (1:1) + 10% FBS. CH22 cells were maintained in RPMI media + 10% FBS. All chordoma cell lines were maintained on collagen I-coated plates. SW 1353 and CAL-78 chondrosarcoma cell lines were obtained from the Broad Institute Cancer Cell Line Encyclopedia project[41]. SW 1353 cells were maintained in DMEM/F12 (1:1) + 10% FBS media. CAL-78 cells were maintained in RPMI media + 20% FBS.

Genome-scale CRISPR-Cas9 screening

Cas9-expressing UM-Chor1 and MUG-Chor1 cells were generated as follows: each parental cell line was incubated with lentivirus corresponding to the pLX_311-Cas9 plasmid (Addgene plasmid #96924), encoding the Cas9 protein, in the presence of 4 μg/mL polybrene, dispensed in 12-well plates (1.5×10^6 cells/well), and spin-infected at 2,000 rpm for 2 h at 30°C. After spin-infection, 2 mL of standard growth media was added to each well, and cells were incubated at 37°C overnight. The following day, for each cell line, cells were trypsinized and expanded in selective media containing blasticidin (2–3 μg/mL for UM-Chor1 and 2 μg/mL for MUG-Chor1). Following selection for infected cells, Cas9 activity was confirmed in each transduced cell line using a previously described Cas9-activity assay[42].

Screening was performed using a genome-scale library of 74,687 unique sgRNAs targeting ~18,560 genes (typically 4 sgRNAs per gene) and 1,000 non-targeting control sgRNAs (Broad Institute Avana sgRNA library)[20]. UM-Chor1-Cas9 and MUG-Chor1-Cas9 cells were each incubated with lentivirus corresponding to the pooled CRISPR library in the presence of 4 μg/mL polybrene, dispensed in 12-well plates (21 plates with 1.5×10^6 cells/well for UM-Chor1 and 15 plates with 3×10^6 cells/well for MUG-Chor1), and spin-infected at 2,000 rpm for 2 h at 30°C. Lentivirus was titered in each cell line to achieve a low MOI (<1), and infections were performed with a sufficient a number of cells to achieve a representation of >800 cells per sgRNA per replicate after selection for infected cells. After spin-infection, 2 mL of standard growth media was added to each well, and cells were incubated at 37°C overnight. The following day, for each cell line, cells were trypsinized, divided into three replicates, and expanded in selective media containing puromycin (3 μg/mL for UM-Chor1 and 6 μg/mL for MUG-Chor1) and blasticidin (3 μg/mL for UM-Chor1 and 2 μg/mL for MUG-Chor1). Cells were grown in culture for 21 d post-infection, with carryover of $>40 \times 10^6$ cells at each passage. Cells were grown in selective media until 7 d (UM-Chor1) or 8 d (MUG-Chor1) post-infection, after which they were grown in standard growth media. At 21 d post-infection, cells were collected and stored at −20°C in PBS until genomic DNA isolation steps.

Genomic DNA was purified from cell pellets using the NucleoSpin Blood XL Kit (Macherey-Nagel). The sgRNA sequence was PCR-amplified with sufficient gDNA to maintain representation and then quantified using massively parallel sequencing[43,44]. For each cell line, primary screening was performed once with three replicates.

CRISPR-Cas9 screening data quality control

Cell lines with poor Cas9 activity (<50%) were excluded from screening. Quality-control measures were used to remove cell line replicate sample data where (1) the single-nucleotide polymorphism (SNP) genotype fingerprint failed to match the reference cell line as previously described[43]; (2) the reproducibility between replicates was less than 70%; (3) the strictly standardized mean difference (SSMD) using positive (proteasome, ribosome, and spliceosome components) and non-targeting controls of fold-change data was poor (>−0.75); and (4) principal component analysis showed a replicate or cell line to be a global outlier of the dataset.

CRISPR-Cas9 data processing and analysis

Data were processed in a reproducible GenePattern pipeline containing individual modules, all available from GParc (gparc.org). Normalized read counts per million were calculated and compared to the abundance of the initial DNA plasmid pool to calculate a $\log_2$ fold change per sgRNA after removing sgRNAs with low abundance in the initial plasmid pool (GP modules: FilterLowPert, PertFoldChange)[43]. The data were batch corrected using the ComBat algorithm to account for a known reagent change during screening (PertBatchCor)[45]. The median of non-targeting controls (n = 1,000) in the Avana library was subtracted from each sgRNA to generate a sgRNA-level score ("sgRNA-dependency score") and plots (NormToNegCntrls, collapseReps). Guides that targeted more than one perfect match location were removed and normalization across cell lines was performed using LOWESS to enable cross-cell-line comparisons (gctRowKeep, NormLines). STARS analysis was performed on LOWESS-normalized sgRNA-level data. The comparison of chordoma and non-chordoma lines was performed using PARIS[43] on LOWESS-normalized sgRNA-level data. The rescaled normalized mutual information (RNMI) score from PARIS was used to rank chordoma selectively essential sgRNAs.

The Mann-Whitney test reported in Fig. 2c was performed in MATLAB (MathWorks, Inc.).

Validation of CRISPR-Cas9 screens

UM-Chor1, MUG-Chor1, and U-CH2 cells were each incubated with lentivirus corresponding to the pXPR_001 plasmid, encoding either sg-*T*#1, sg-*T*#2, or sg-*EGFP* (sequences below), in the presence of 4 μg/mL polybrene, dispensed in 12-well plates (1.5 × 10^6 cells/well for UM-Chor1 and MUG-Chor1, 1.2×10^6 cells/well for U-CH2), and spin-infected at 2,000 rpm for 2 h at 30°C. After spin-infection, 2 mL of standard growth media was added to each well, and cells were incubated at 37°C overnight. The following day, for each cell line, cells were trypsinized and expanded in selective media containing puromycin (2 μg/mL for UM-Chor1, 1–2 μg/mL for MUG-Chor1, 3 μg/mL for U-CH2). Following selection for infected cells, cells were seeded in 24-well plates in selective media (30,000 cells/well for UM-Chor1 and U-CH2 and 40,000 cells/well for MUG-Chor1, with three replicates per timepoint), and counted at indicated intervals over a 25 d period. In parallel, selected cells were harvested (at least 9 d post-transduction) for immunoblotting to confirm sgRNA-mediated protein reduction. Proliferation experiments were performed twice for UM-Chor1 and U-CH2 with minor modifications between experiments and once for MUG-Chor1, with three replicates per experiment. Immunoblots were performed once. Statistical analysis was performed with GraphPad Prism v7.

Lentiviral vectors used for screening validation and functional characterization

The *T*-targeting sgRNAs used for low-throughput experiments were cloned in the pXPR_001 lentiviral vector, which encodes the Cas9 protein[46]. Spacer sequences for *T*-targeting sgRNAs were as follows: sg-*T*#1, CCCTGAGACCCAGTTCATAG; sg-*T*#2, TGGCTGGTGATCATGCGCTG. The pXPR_001 plasmid encoding sg-*EGFP* was provided by the laboratory of Feng Zhang (Broad Institute, Cambridge, MA) and has been described previously ("EGFP sgRNA 6")[46]. Lentivirus was produced by transfection of 293T packaging cells with three plasmids [pXPR_001-sgRNA, 8.9 (*gag*, *pol*), and VSV-G]; and

the FuGene6 transfection reagent (Roche). Virus-containing supernatant was harvested 3 d post-transfection.

Small-molecule sensitivity profiling

Chemical sensitivity tests similar to those reported in the Cancer Therapeutics Response Portal (CTRP: www.broadinstitute.org/ctrp/) were performed using 459 small molecules chosen collectively to target a diverse set of nodes in cell circuitry, and with a high degree of overlap to published informer sets (Supplementary Table 2)[22], including 428 compounds published in CTRP. UM-Chor1, MUG-Chor1, U-CH1, and JHC7 cells were each seeded overnight in 384-well BioCoat Collagen I (Corning) microtiter plates at a density of 1200, 1800, 2000, and 1600 cells per well, respectively. The following day, compound or DMSO was added to wells (1:400 dilution) using a CyBio pinning instrument. Each compound was tested using 8 concentrations in duplicate. Cells were incubated at 37°C, and cell viability was assayed 6 d after the addition of compound or DMSO using the CellTiter-Glo reagent (Promega). For each cell line, primary screening was performed once with two replicates.

Computational analysis software for small-molecule sensitivity studies

Computational analyses and visualizations were performed in Microsoft Excel Professional Plus 2013, GraphPad Prism (v6 or v7), Pipeline Pilot (version 8.5) (Accelrys, Inc.), or MATLAB 8.4 (2014b) or MATLAB 9.4 (2018a) (MathWorks, Inc.), as described in the following specific Methods sections.

Identification of candidate antiproliferative small molecules in chordoma

The response of each chordoma cell line to a tested compound was quantified as follows: log-transformed duplicate data were averaged during normalization of luminescence values to vehicle (DMSO) treatment[47], and at each compound concentration, an average percent-viability (PV) score was calculated. PV response-point measurements were computed across all cell lines, compounds, and concentrations. Curves were fit with nonlinear sigmoid functions, and the area-under-curve (AUC) for each CCL-compound pair was calculated by numerically integrating under the 8-point concentration-response curve essentially as described previously[22]. In our analysis, we differed from the published procedure in (1) the number of concentrations tested; (2) the use of fixed concentration limits of integration for AUCs across all compounds; (3) standardization of AUC values on the range from 1 (DMSO or no effect) to 0 (complete killing throughout the concentration range of integration); *cf.* https://github.com/remontoire-pac/ctrp-reference/tree/master/auc. Data pre-processing from instrument files through DMSO normalization was performed in Pipeline Pilot, and curve-fitting, numerical integration, and subsequent analysis steps were performed in MATLAB.

To identify candidate antiproliferative small molecules in chordoma, a threshold was applied to include only potent compounds (average AUC across four chordoma cell lines < 0.8). Next, to assess whether a compound had selectively cytotoxic effects in chordoma lines relative to other cell lines tested in CTRP, we computed the median AUC for 4 chordoma lines and z-scored this median with respect to the mean and standard deviation of all other cell lines tested with that compound. We applied this selectivity analysis to filter out potent compounds whose cytotoxic effects were non-selective for chordoma cell lines (z-score <

−1), when those data were available. We note that some compounds were only tested in the chordoma lines, and therefore data about their performance across CTRP lines were not available; in such cases, we did not apply any additional filtering step beyond the initial potency filter. Twenty-eight compounds passed these criteria, and 431 compounds were filtered out. Compounds targeting proteins of interest (CDK 7,12,13,9 and EGFR/ERBB2) were carried forward for secondary screening.

Validation of small-molecule sensitivity screens

UM-Chor1, MUG-Chor1, U-CH1, JHC7, and CH22 cells were each seeded overnight in 384-well BioCoat Collagen I (Corning) microtiter plates at a density of 1200, 1800, 2000, 1600, and 1200 cells per well, respectively. The following day, compound or DMSO was added to wells using an HP D300 digital dispenser instrument. Each compound was tested using 9 concentrations, in quadruplicate (four wells treated in parallel). Cell viability was assayed 6 d after compound addition with the CellTiter-Glo reagent (Promega). Luminescence values were treated as with the primary screening data (*vide supra*). Data pre-processing from instrument files through DMSO normalization was performed in Pipeline Pilot for UM-Chor1, MUG-Chor1, U-CH1, JHC7, or Microsoft Excel for CH22; and curve-fitting, numerical integration, and subsequent analysis steps were performed in MATLAB. Experiments depicted in Fig. 2b, Extended Data Fig. 2a, and Extended Data Fig. 3a were performed at least twice in each cell line (except afatinib treatment in JHC7 cells, which was performed once); experiments depicted in Extended Data Fig. 8c were performed at least three times in UM-Chor1 cells and once for all other cell lines. Experiments depicted in Extended Fig. 10a were performed once. For experiments performed multiple times, compound addition was performed using either a digital dispenser instrument, as described above, or a Cybio pinning instrument.

Small-molecule reagents

Small molecules used for low-throughput *ex vivo* experiments were obtained from the following sources: THZ1, THZ531, and NVP-2 were provided by the laboratory of Nathanael Gray (Dana-Farber Cancer Institute; Boston, MA); JQ1 was provided by the laboratory of James Bradner (Dana-Farber Cancer Institute; Boston, MA); CCT251545 was provided by Paul Clarke and Aurelie Mallinger (The Institute of Cancer Research; London, UK); alvocidib, AT7519, dinaciclib, LEE011, and palbociclib were purchased from Selleck Chemicals; erlotinib and dasatinib were purchased from LC Laboratories; actinomycin D was purchased from Gibco; neratinib, canertinib, lapatinib, and afatinib were obtained from Broad Institute Compound Management and were originally purchased from Selleck Chemicals; BRD6989 was obtained from Broad Institute Compound Management and was originally purchased from Vitas-M Laboratory (cat# STL241555). Small molecules used for high-throughput screening were obtained from Broad Institute Compound Management (Broad Institute Compound IDs reported in Supplementary Table 2). THZ1 Hydrochloride used for *in vivo* studies was purchased from MedChemExpress.

RNA-sequencing

For RNA-sequencing experiments with sgRNA-treated cells: UM-Chor1 cells were incubated with lentivirus corresponding to the pXPR_001 plasmid, encoding either sg-*T*#1,

sg-*T*#2, or sg-*EGFP* in the presence of 4 μg/mL polybrene, dispensed in 12-well plates (1.3 × 10^6 cells/well), and spin-infected at 2,000 rpm for 2 h at 30°C. After spin-infection, 2 mL of standard growth media was added to each well, and cells were incubated at 37°C overnight. The following day, cells were trypsinized and expanded in selective media containing puromycin (2 μg/mL). Following selection for infected cells, selective media was replaced with standard growth media, and cells were harvested 2 d later. Cell pellets were used for RNA extraction using an RNeasy Kit (Qiagen). Sequencing libraries were prepared using the NEBNext Ultra Directional RNA Library Prep Kit for Illumina (New England BioLabs), and libraries were sequenced using the Illumina HiSeq 2500 instrument (rapid-run mode) with paired-end 100 bp reads. Sequencing was performed once with two biological replicates for each condition.

For RNA-sequencing experiments with compound-treated cells: UM-Chor1 cells were seeded overnight in 6 cm collagen I-coated dishes at a density of 750,000 cells per dish. The following day, media was replaced with standard growth media containing compound at the final concentration or DMSO. Compound- and DMSO-treated cells were harvested 4 h after compound or DMSO addition. Cell pellets were used for RNA extraction using an RNeasy Kit (Qiagen). Sequencing libraries were prepared using the TruSeq Stranded mRNA Library Prep Kit (Illumina), and libraries were sequenced using the Illumina NextSeq 500 instrument with single-end, 75 bp reads. Sequencing was performed once with two biological replicates for each condition.

RNA-sequencing analysis

For all RNA-seq experiments, raw reads were processed with Trim Galore! (version 0.4.1) (Babraham Bioinformatics; https://www.bioinformatics.babraham.ac.uk/projects/trim_galore) to remove adapter sequences and aligned with STAR (version 2.4.2)[48] to the human genome (GRCh38, primary assembly) using the GENCODE annotation (version 23). Differential expression analysis was performed in R (version 3.2.1) (http://www.R-project.org/) using the DESeq2 package (version 1.10.0)[49].

Gene set enrichment analysis was performed with GSEA2 (version 2.2.0) and gene sets from MSigDB (version 5.0)[50,51]. We used the "preranked" algorithm to analyze gene lists ranked by the negative decadic logarithm of adjusted p-values obtained from the differential-expression analysis with DESeq2. To separate up- and down-regulated genes, we artificially assigned a negative sign to values for downregulated genes (thus using the decadic logarithm of adjusted p-values). We used the options –nperm 1000, -set_max 1500, and –set_min 5.

Copy number variation analysis

Whole-exome sequencing data for all chordoma cell lines were obtained from the Chordoma Foundation (available at www.cavatica.org) and processed according to the GATK Best Practices[52]. Briefly, starting with reads in an unaligned BAM file, we marked sequencing adapters with Picard (version 1.999) MarkIlluminaAdapters, aligned reads to the human genome (hg19) with BWA (version 0.7.12)[53], and marked duplicates with Picard MarkDuplicates (Broad Institute Picard; https://github.com/broadinstitute/picard). We then used the GATK3 toolkit (version 2.2) to perform Indel Realignment and Base Recalibration

(Broad Institute GATK; software.broadinstitute.org/gatk)[54]. Somatic copy number variations were determined using the GATK4 toolkit (Broad Institute GATK; https://gatkforums.broadinstitute.org/gatk/discussion/9143/how-to-call-somatic-copy-number-variants-using-gatk4-cnv).

RT-qPCR

RT-qPCR of compound-treated cells—UM-Chor1 cells were seeded overnight in 6-well collagen I-coated dishes at a density of 275,000 cells per well. The following day, media was replaced with standard growth media containing compound at the final concentration or DMSO. Compound- and DMSO-treated cells were harvested 4, 8, and 12 h after compound or DMSO addition, and cell pellets were used for RNA extraction using an RNeasy Kit (Qiagen). Three biological replicates were generated per condition. Total RNA was reverse transcribed to cDNA using the High-Capacity RNA-to-cDNA Kit (Applied Biosystems). cDNA was used for qPCR using the Taqman Gene Expression Master Mix and Taqman Gene Expression probes (Applied Biosystems). For each cDNA sample, four technical replicate reactions were performed using probes for the gene of interest, and, in parallel, for the *GAPDH* reference gene. The Taqman probes used in the study were as follows: *T*, hs00610080_m1; *MAX*, hs00811069_g1; *CFL1*, hs02621564_g1; *GAPDH*, hs02758991_g1. Amplification was performed using the QuantStudio 6 Flex instrument (Applied Biosystems). The experiment was performed twice with variations in cell seeding density and replicate numbers, with similar conclusions.

RT-qPCR of sgRNA-treated cells—UM-Chor1 cells were transduced with sgRNAs targeting *T* and *EGFP* and subjected to RNA extraction as described in the RNA sequencing methods section. Total RNA was used for cDNA synthesis and qPCR, with four technical replicates per qPCR reaction condition, as described above. The Taqman probes used in the study were as follows: *T*, hs00610080_m1; *GAPDH*, hs02758991_g1; *ATP6V1B2*, hs00156037_m1; *SAE1*, hs00271440_m1; *SOX9*, hs00165814_m1; *TPX2*, hs00201616_m1. The experiment was performed once with two biological replicates for each sgRNA.

Analysis of RT-qPCR data—RT-qPCR data were analyzed according to the instrument manufacturer's instructions for relative quantity (RQ) calculations using the $\Delta\Delta C_T$ method. For each sample, cycle threshold (C_T) values were averaged across technical replicates. ΔC_T values were then calculated by subtracting the average reference-gene (GAPDH) C_T values from average target-gene C_T values, for each biological replicate. We applied a one-sided Welch's t-test comparing ΔC_T values for treatment and reference samples to determine significant differences. Log$_2$-fold-changes were calculated as $\Delta\Delta C_T$ values by subtracting ΔC_T values for the reference samples from ΔC_T values for the treated samples. All calculations were done in R (version 3.4.4).

Caspase-3/7 activity assay

UM-Chor1 cells were seeded overnight in 384-well BioCoat Collagen I (Corning) microtiter plates at a density of 1200 cells per well. The following day, THZ1 or DMSO was added to wells using a HP D300 digital dispenser instrument. Cells were incubated at 37°C, and

caspase-3/7 activity and cell viability were assayed in parallel 24 h and 48 h after the addition of compound or DMSO using the Caspase-Glo 3/7 and CellTiter-Glo reagents, respectively (Promega). Four replicate wells were treated per condition. Luminescence values corresponding to compound-treated cells were normalized to those of DMSO-treated cells to calculate relative caspase-3/7 activity or relative cell viability. The experiment was performed twice.

Compound or sgRNA treatment for immunoblot analysis

For Fig. 4a: MUG-Chor1 and UM-Chor1 cells were seeded overnight in 6 cm collagen I-coated dishes at a density of 750,000 cells per dish. The following day, media was replaced with standard growth media containing compound at the final concentration or DMSO. Cells were harvested 48 h after compound or DMSO addition and cell pellets were used for immunoblot analysis. The experiment was performed four times for UM-Chor1 with variations in compound concentration and incubation times, with similar conclusions, and once for MUG-Chor1.

For Fig. 4b and Extended Data Fig. 10b: MUG-Chor1, UM-Chor1, U-CH1, JHC7, and CH22 cells were each seeded overnight in 6 cm collagen I-coated dishes at a density of 750,000 cells per dish. The following day, media was replaced with standard growth media containing compound at the final concentration or DMSO. Cells were harvested 48 h after compound or DMSO addition, and cell pellets were used for immunoblot analysis. The experiment was performed two times for MUG-Chor1, UM-Chor1, and U-CH1, with variations in compound concentration and incubation times, with similar conclusions, and once for JHC7 and CH22.

For Extended Data Fig. 8a: UM-Chor1 cells were seeded overnight in 6 cm collagen I-coated dishes at a density of 750,000 cells per dish. The following day, media was replaced with standard growth media containing compound at the final concentration or DMSO. Cells were harvested 12 h, 24 h, 36 h, and 48 h after compound or DMSO addition and cell pellets were used for immunoblot analysis. The experiment was performed once.

For Fig. 2d and Extended Data Fig. 3b: UM-Chor1 cells were seeded overnight in 6 cm collagen I-coated dishes at a density of 750,000 cells per dish. The following day, media was replaced with standard growth media containing compound at the final concentration or DMSO. Cells were harvested 24 h after compound or DMSO addition, and cell pellets were used for immunoblot analysis. The experiment was performed 2 times for THZ1, with minor variations in compound concentrations, with similar conclusions, and CCT251545; and once for other compounds.

For Extended Data Fig. 9b, UM-Chor1 cells were transduced with sgRNAs targeting *T* and *EGFP* and used for immunoblotting as described in the methods section describing validation of CRISPR-Cas9 screens. Transductions were performed once; immunoblots were performed twice.

Immunoblotting

Cell pellets were resuspended in lysis buffer (50 mM Tris pH 7.4, 2.5 mM EDTA pH 8, 150 mM NaCl, 1% Triton X-100, 0.25% IGEPAL CA-630) containing protease inhibitors (Roche) and Phosphatase Inhibitor Mixtures I and II (Calbiochem). Lysates were incubated on ice for >2 min, then centrifuged for 2 min at 15,700 x g. Supernatants were quantified using a BCA Protein Assay Kit (Pierce), normalized, reduced, and denatured. Protein samples were then resolved using Tris-Glycine gels (Novex), and resolved protein was transferred to iBlot Transfer Stack nitrocellulose membranes (Novex). Membranes were probed with primary antibodies at 4°C overnight. The antibodies against brachyury (clone N-19, #sc-17743; 1:1,000) and CDK7 (clone C-4, #sc-7344, 1:1,000) were purchased from Santa Cruz Biotechnology. Antibodies against cofilin (clone D3F9, #5175; 1:10,000), total Rb (clone 4H1, #9309; 1:2,000), phospho-Rb S807/S811 (clone D20B12, #8516; 1:1,000), phospho-Rb S780 (clone D59B7, #8180; 1:1,000), SOX9 (clone D8G8H, #82630, 1:1,000), total STAT1 (clone 9H2, #9176; 1:1,000), and phospho-STAT1 S727 (clone D3B7, #8826; 1:1,000) were purchased from Cell Signaling Technology. Antibodies against phospho-POLR2A Ser2 (clone 3E1, #04–1571-I; 1: 1,000), phospho-POLR2A Ser5 (clone 3E8, #04–1572-I; 1:1,000), and phospho-POLR2A Ser7 (clone 4E12, #04–1570-I; 1:1,000) were purchased from Millipore. The antibody against total POLR2A (#A300–653A; 1:400) was purchased from Bethyl Laboratories. The antibody against the V5 tag (#46–0705, 1:5,000) was purchased from Invitrogen. Membranes were incubated with IRDye secondary antibodies (1:10,000; LI-COR Biosciences) and detected with the Odyssey Imaging System (LI-COR Biosciences). Immunoblots were quantified by densitometry, typically using the predominant band species, with ImageJ software (NIH). Quantification results appear in Supplementary Table 10.

Patient-derived chordoma tumor and normal adjacent tissue samples

Patient-derived tumor and normal adjacent tissue specimens from Massachusetts General Hospital (MGH) were obtained from the clinical archives of Dr. Francis Hornicek (Department of Orthopaedic Surgery, Massachusetts General Hospital). Institutional review board (IRB) approval was obtained to study these tumor samples via Dana-Farber/Harvard Cancer Center protocol number 03–344. Patients were consented according to protocol. Following resection, tissue was flash frozen and stored at –80°C until later use.

Patient-derived tumor specimens from the Chordoma Foundation (CF) Biobank were collected under the CF's IRB-approved protocol QR26112/1. Patients gave their written informed consent for scientific study of their tumor cells. Following resection, tissue was flash frozen and stored in liquid nitrogen or –80°C until later use for ChIP-seq. Immunohistochemistry was performed as described below.

Studies were in compliance with all relevant ethical regulations.

Immunohistochemical staining for brachyury expression

Staining was performed by the Histology Core Facility at Ohio State University. Slides were cut from FFPE blocks of patient tissue and were heated at 75°C for 15 min, then dewaxed in xylene and graded alcohols as follows: xylene, 5 min (2X); 100% ethanol, 5 min (2X); 95%

ethanol, 2 min; 70% ethanol, 2 min; 50% ethanol, 2 min; distilled water, 2 min. Antigen retrieval was performed by steaming in citric acid pH 6 (10 mM) for 15 min. Slides were cooled for 15 min, then washed with water for 5 min. Slides were blocked with hydrogen peroxide 3% for 15 min at RT then washed with water for 5 min, followed by a quick PBS wash. Slides were incubated with blocking buffer for 30 min at RT (Dako, #X0909), followed by incubation with the brachyury antibody (Santa Cruz Biotechnology, #sc-17743, 1:150) overnight at 4°C. Slides were washed with PBS 3 X 5 min, then incubated with secondary antibody (Cell IDx, #GH-015) for 1h at 37°C. Slides were washed with PBS 3 X 5 min. Stains were developed using DAB, then washed with PBS 3 X 5 min. Counterstaining was performed with hematoxylin. Tissue sections were dehydrated with graded alcohols as follows: 50% ethanol, 2 min; 70% ethanol, 2 min; 95% ethanol, 2 min; 100% ethanol, 2 min (2X); xylene, 5 min (2X). Slides were mounted using Cytoseal (Richard-Allan Scientific).

Images were converted to high-resolution digital images using Leica ScanScope XT. Images were visualized for figures using Aperio ImageScope software.

Chromatin immunoprecipitation (ChIP)

For H3K27ac ChIP of patient-derived tissue: approximately 100 mg of flash-frozen tissue was minced into 1–2 mm pieces and incubated in 1% formaldehyde for 15 minutes, followed by quenching with glycine (125 mM final concentration). Fixed tissue pieces were homogenized with a Tissue Tearor rotor stator homogenizer (Biospec) set to 30,000 RPM for 60 seconds. Homogenate was washed with ice-cold PBS containing 1X HALT protease inhibitor. Homogenized pellets were then resuspended in cytosolic lysis buffer (50 mM HEPES pH 7.5, 140 mM NaCl, 1 mM EDTA, 10% glycerol, 0.5% IGEPAL, 0.25% Triton X-100, 1X HALT protease inhibitor) and the protocol was continued as described below.

For H3K27ac ChIP of chordoma cell lines: Chordoma cell lines were grown in 175 cm collagen I-coated plates (3 plates per cell line) and cross-linked by adding 1/10 of the cell culture volume of 11% formaldehyde solution (1M HEPES-KOH pH 7.5, 0.5 M EDTA pH 8.0, 0.5 M EGTA pH 8.0, 5 M NaCl, 37% formaldehyde) for 10 minutes, followed by quenching (125 mM glycine). Cells were washed in PBS and harvested by cell scraper in PBS. Cells were centrifuged at 1,350 X g for 5 min at 4°C, washed with PBS, and centrifuged again at 1,350 X g for 5 min at 4°C. Cell pellets were flash frozen and stored at −80°C until further processing.

For both cell line and tissue ChIP-seq: samples were subsequently rotated end-over-end for 10 minutes at 4º C in cytosolic lysis buffer and then collected by spinning at 1,350 x g for 5 minutes. Samples were resuspended in nuclear lysis buffer (10 mM Tris-HCl pH 8, 200 mM NaCl, 1 mM EDTA, 0.5mM EGTA, 1X HALT protease inhibitor) and rotated end-over-end for 10 minutes at 4º C and spun at 1,350 x g for 5 minutes. Samples were resuspended in 1 mL sonication buffer (0.1% Na-Deoxycholate, 50 mM HEPES pH 7.5, 140 mM NaCl, 1 mM EDTA, 1 mM EGTA, 1% Triton X-100, 1X HALT protease inhibitor) with SDS added to a final concentration of 0.5%. Chromatin was sheared by sonication using a Bioruptor water bath sonicator (Diagenode) for 25 cycles. Samples were clarified by centrifuging 10 minutes at 20,000 x g at 4º C. A 50 uL aliquot of supernatant was set aside

as non-IP input control. The remaining sheared chromatin was diluted 1:5 in sonication buffer and each sample was incubated overnight at 4º C with 100 uL of Protein G Dynabeads (Life Technologies) bound with 10 µg of anti-H3K27ac antibody (abcam, #ab4729). Beads were washed while rotating end-over-end at 4º C with the following buffers: twice in sonication buffer, once in sonication buffer with NaCl added to a final concentration of 500 mM, once in LiCl wash buffer (20 mM Tris pH 8, 1 mM EDTA, 250 mM LiCl, 0.5% IGEPAL, 0.5% Na-Deoxycholate), and once in TE-NaCl buffer (50 mM Tris-HCl pH 8, 50 mM NaCl). Chromatin was eluted by resuspending beads in 200 uL elution buffer (50 mM Tris-HCl pH 8, 10 mM EDTA, 1% SDS) and heating for 15 minutes at 65º C. Beads were pelleted by centrifuging at 20,000 G for 30 seconds and supernatant was collected. Elution buffer (150 uL) was also added to input chromatin samples. Samples were incubated at 65º C overnight to reverse crosslinks. Samples were then incubated with RNAse A (Thermo Scientific) for 2 hours at 37º C, followed by incubation with Proteinase K (Ambion) for 30 minutes at 55º C. DNA isolation was performed via phenol-chloroform extraction and concentrated by ethanol precipitation. Sequencing libraries were generated with the Thruplex DNAseq Single Index Kit (Rubicon) and sequenced on an Illumina NextSeq 500 with single-end, 75 bp reads. ChIP-seq was performed once for each sample.

Assay for transposase-accessible chromatin (ATAC)

For each cell line (MUG-Chor1 and U-CH2), 50,000 cells were lysed for 10 minutes at 4°C in lysis buffer (10 mM Tris-HCl pH 7.4, 10 mM NaCl, 3 mM $MgCl_2$, 0.1% IGEPAL CA-360). After lysis, the pellets were subject to a transposition reaction (37°C, 60 minutes) using the 2X TD buffer and transposase enzyme (Illumina Nextera DNA preparation kit, FC-121–1030). The transposition mixture was purified using a Qiagen MinElute PCR purification kit. Library amplification was performed using custom Nextera primers and the number of total cycles determined by running a SYBR-dye based qPCR reaction and calculating the cycle number that corresponds to ¼ the maximum. Amplified libraries were purified using a Qiagen PCR purification kit and sequenced with paired-end 100 bp reads on an Illumina HiSeq 2000. ATAC-seq was performed once for each cell line, with two biological replicates for U-CH2 and one replicate for MUG-Chor1.

ChIP-seq data analysis

Genomic coordinates and gene annotation.—All coordinates and gene annotations in this study were based on human reference genome assembly hg19, GRCh37 (ncbi.nlm.nih.gov/assembly/2758/) and RefSeq genes.

ChIP-seq data processing.—All datasets were aligned using Bowtie2 (version 2.2.1) to build version NCBI37/HG19[55]. Alignments were performed using all default parameters except for –N 1.

Calculating read density.—We calculated the normalized read density of a ChIP-seq dataset in any genomic region using the Bamliquidator (version 1.0) read density calculator (https://github.com/BradnerLab/pipeline/wiki/bamliquidator). Briefly, ChIP-seq reads aligning to the region were extended to 200 bp and the density of reads per base pair (bp) was calculated. The density of reads in each region was normalized to the total number of

million mapped reads producing read density in units of reads per million mapped reads per bp (rpm/bp).

Plotting composite representations of ChIP-seq signal at individual loci.—To compactly display ChIP-seq signal from multiple cell line or patient-derived chordoma samples at individual genomic loci samples, we developed a simple meta representation as previously described[35]. For all samples within a group, ChIP-seq signal is smoothed using a simple spline function and plotted as a translucent shape in units of rpm per bp. Darker regions indicate regions with signal in more samples. An opaque line is plotted and gives the average signal across all samples in a group.

Identifying enriched regions.—We used the MACS version 1.4.2 (model-based analysis of ChIP-seq) peak finding algorithm to identify regions of ChIP-seq enrichment over background[56]. A p-value threshold of enrichment of 1e-9 was used for all datasets.

Defining active genes.—Across chordoma cell lines, active genes were defined as those with an enriched H3K27ac region in at least one cell line in the +/− 1kb region flanking the transcription start site (TSS).

Mapping typical enhancers and super-enhancers using H3K27ac enhancer definitions in individual samples.—H3K27ac super-enhancers (SEs) and typical enhancers (TEs) in individual chordoma samples were mapped using the ROSE2 software package described previously[57] and available at https://github.com/BradnerLab/pipeline - ROSE2_main.py. For each dataset, a stitching parameter was determined that consolidated proximal peaks while optimizing the enriched fraction of stitched peaks. Peaks contained within the +/− 2.5 kb flanking the transcription start site of genes were excluded (-t 2500 parameter). To assign enhancers to the *T* or *MAX* genes, a 100 kb proximity window was used (Extended Data Figs. 4 and 6).

Mapping typical enhancers and super-enhancers using H3K27ac enhancer definitions across composites of cell lines or patient-derived chordoma samples.—H3K27ac super-enhancers (SEs) and typical enhancers (TEs) composite landscapes in either chordoma cell lines or patient-derived samples were mapped using the ROSE2 software package described previously[57] and available at https://github.com/BradnerLab/pipeline - ROSE2_META.py. Briefly, for a given cohort of samples (e.g. cell lines), the union of all discrete H3K27ac enriched regions was determined. For each cohort of samples, a stitching parameter was determined that consolidated proximal peaks while optimizing the enriched fraction of stitched peaks. The average background subtracted signal for each sample across a cohort was averaged and used to rank enhancers. To assign enhancers to all genes, a 50 kb proximity window was used. Across chordoma cell lines, we identify a total of 1,199 SEs (Fig. 3e and Supplementary Table 5). Across patient-derived chordoma samples, we identified 1,490 SEs (Fig. 3g and Supplementary Table 7). Locations, ranks, proximal and overlapping genes for composite chordoma cell line and patient-derived sample SEs are provided in Supplementary Tables 5 and 7.

Quantifying expression of SE-associated transcription factors.—Cell line expression data were provided by the Chordoma Foundation (available at www.cavatica.org). Briefly, reads were aligned with STAR aligner and quantified with Sailfish to produce expression measurements in units of transcripts per million (tpm). We selected all genes that were (1) associated with SEs in chordoma cell lines, (2) expressed (>1 tpm in at least 1 sample), and (3) annotated as transcription factors in UniProt, resulting in 115 genes. Gene-expression levels for the top 30 SE-associated TFs, ranked by mean expression, are shown in Fig. 3d; levels for all 115 genes are shown in Extended Data Fig. 5c.

Clustering ChIP-seq samples.—To cluster ChIP-seq samples by similarity of H3K27ac enhancer profiles, we first defined the union of all enhancer regions present in any individual chordoma sample. ChIP-seq signal was calculated at all regions, background subtracted, and then median normalized. Samples were then clustered using hierarchical clustering of cross sample Pearson correlation (Fig. 3j).

ATAC-seq data analysis

All paired-end datasets were aligned using Bowtie2 (version 2.2.1) to build version NCBI37/ HG19 with the following parameters: -k 1. Aligned bams were filtered and sorted using samtools (0.1.19) by removing chrM and duplicate reads, and filtering against the ENCODE blacklist (https://sites.google.com/site/anshulkundaje/projects/blacklists). Peaks were called using MACS version 1.4.2 with a p-value cutoff of 1e-9.

ORF rescue experiments

For cell viability experiments, UM-Chor1 cells were seeded overnight in 384-well BioCoat Collagen I (Corning) microtiter plates at a density of 1000 cells per well. The following day, cells were incubated with lentivirus corresponding to the pLX-Blast-V5 expression vector[58] encoding either the *LACZ* or *T* (p.Gly177Asp variant)[12] ORF in the presence of 4 μg/mL polybrene, spin-infected at 1,126 × g for 30 min at 30 °C, then incubated at 37 °C for an additional 4.5 – 5.5 h before replacing media with standard growth media. Three days post-infection, cells were treated with 500 nM THZ1 (12 replicate wells treated in parallel) or DMSO (8 replicate wells treated in parallel) using a using an HP D300 digital dispenser instrument. Cell viability was assayed 6 d after the addition of THZ1/DMSO using the CellTiter-Glo reagent (Promega). Infection efficiency was assayed in a parallel experiment by adding 3 μg/mL blasticidin to infected wells one day post-infection. The experiment was performed three times. Statistical analysis was performed with GraphPad Prism v7.

For the immunoblot experiment depicted in Fig. 4d, UM-Chor1 cells were seeded overnight in 6-well collagen I-coated plates at a density of 300,000 cells per well. The following day, cells were treated with lentivirus corresponding to the pLX-Blast-V5 expression vector encoding either the *LACZ* or *T* (p.Gly177Asp variant) ORF in the presence of 8 μg/mL polybrene, and incubated at 37 °C for ~19–20 h before replacing media with standard growth media. The following day, media was replaced with selective media containing blasticidin (4 μg/mL). Following selection for infected cells (at least 7 d later), media was replaced with standard growth media containing compound at the final concentration or

DMSO. Cells were harvested 48 h after compound or DMSO addition, and cell pellets were used for immunoblot analysis. The experiment was performed twice.

STARS and integrative analyses

STARS, an algorithm designed to rank genes in genetic perturbation screens (https://portals.broadinstitute.org/gpp/public/software/stars), was used to identify significantly essential genes in each chordoma line screened. sgRNAs were ranked by the sgRNA-dependency score in each line, then STARS was run at a 5% threshold to ensure that at least 2 independent sgRNAs scored for each gene in the top 5% of all sgRNAs screened. Genes scored as essential in each line, if they passed these criteria. For Fig. 4f, those genes scoring in each chordoma cell line were then intersected with the list of expressed, super-enhancer-associated genes in the same cell line. Gene-expression levels in each cell line were assessed using RNA-sequencing data, which was obtained from the Chordoma Foundation (available at www.cavatica.org), and processed as described in the RNA-sequencing analysis methods. H3K27ac super-enhancers (SEs) in individual chordoma cell lines were mapped as described in the ChIP-seq data analysis methods section, except that we used a (higher confidence) 50 kb proximity window to assign enhancers to genes. For a gene to be considered downregulated by sg-T#1 and sg-T#2 in Fig. 4f, the relative gene expression (as measured by RNA-sequencing) of cells transduced with sg-T versus a non-targeting control must have had a $\log_2$-fold change < 0 and an adjusted p-value < 0.01. Brachyury ChIP-seq analysis was performed as described in the associated methods section.

Brachyury ChIP-seq analysis

We obtained FASTQ files for a previously reported brachyury ChIP-seq experiment[33]. We aligned ChIP-seq reads to the human reference genome (hg19) using Bowtie 2 (version 2.2.1)[55] and converted the aligned BAM files to BED files using BEDtools (version 2.26.0)[59]. Peaks were then called with MACS (version 1.4.2)[56] and annotated with nearby genes using HOMER (version 4.9.1) (http://homer.ucsd.edu/homer/)[60]. To be demarcated with a cross in Fig. 4f, a gene must have been associated with a peak passing the significance threshold ($p < 0.05$) in all three ChIP-seq replicates.

In vivo treatment studies

All breeding, mouse husbandry, and *in vivo* experiments were performed with the approval of the NYU Langone Medical Center (NY, NY) Animal Care and Use Committee.

SCID Hairless Outbred (SHO), all female, 6–8 week-old mice were purchased from Charles River Laboratories International Inc. (#474). CH22 cells were cultured in RPMI media + 10% FBS on collagen I-coated 175 cm^2 flasks (Corning). Cells were resuspended in serum-free medium mixed with an equal amount of Matrigel (Corning, #354234). For the study depicted in Fig. 4h–i and Extended Data Fig. 10e (bottom panel): mice were injected with 8 million cells per shot and 2 locations per mouse in the flanks. The mice were randomly grouped. Each cohort included 10 mice. Treatment was started when the mean tumor size per group reached approximately 500 mm^3. Three mice of each group were taken out on Day 3 for target engagement analysis. One mouse in the vehicle group did not have tumor engrafted and was therefore excluded from the study. Tumor sizes were monitored

weekly, and volumes were calculated with the following formula: (mm^3) = length × width × width × 0.5.

THZ1 was dissolved in DMSO:5% dextrose (1:10) and dosed as 40 mg/kg twice daily via the intraperitoneal route. Vehicle-group mice received DMSO:5% dextrose (1:10) via the same route. The dosing schedule for the first week was continuous dosing for the first three days; for subsequent weeks, animals were dosed three times a week, on alternating days, as depicted in Fig. 4h. Statistical analysis was performed with GraphPad Prism v7. The efficacy study was performed once.

For the experiments depicted in Extended Data Fig. 10d and Extended Data Fig. 10e (top panel), injections and compound treatment were performed in a similar fashion as the target engagement study described above, except that the experiment depicted in Extended Data Fig. 10d was performed for 5 d and had an additional treatment arm of 20 mg/kg THZ1 twice daily. Each of the three target engagement studies reported was performed once.

For immunoblotting of tumor tissue, tumor fragments were homogenized in lysis buffer (recipe described in the immunoblotting methods section) using the Precellys Evolution (Bertin Technologies) instrument (3 × 7500 rpm for 20 s, pausing for 15 s between rounds). Homogenized lysates were centrifuged for 2 min at 15,700 x g. Supernatants were quantified and used for immunoblotting as described in the immunoblotting methods section. Immunoblots were performed once.

Studies were in compliance with all relevant ethical regulations.

Code availability

Computational code used for ChIP-seq analysis can be found at github.com/linlabcode/ chordoma_code. Code for CRISPR-Cas9 screening analysis is available on GParc (www.gparc.org). Code for small-molecule sensitivity profiling analysis; and DNA and RNA sequencing analysis are available upon reasonable request.

Data availability

CRISPR-Cas9 screening data for two chordoma cell lines (pertains to Figs. 1, 2, 4, and Extended Data Fig. 1) are available at Figshare (DOI: 10.6084/m9.figshare.7302515). CRISPR-Cas9 screening data for all other cancer cell lines (pertains to Figs. 1, 2, 4, and Extended Data Fig. 1) were generated as part of Project Achilles (Broad Institute Project Achilles; https://depmap.org/portal/achilles/). All RNA-sequencing data (pertains to Figs. 1 and 4) are available at Gene Expression Omnibus (GEO) (accession number: GSE121846). Small-molecule sensitivity data generated using non-chordoma cell lines and used for comparative analyses (pertains to Fig. 2) are available at the National Cancer Institute's CTD^2 Data Portal (https://ocg.cancer.gov/programs/ctd2/data-portal) and the CTRP (www.broadinstitute.org/ctrp/). The analysis of new small-molecule primary screening data generated using chordoma cell lines (pertains to Fig. 2) was performed as described previously[22], except as noted in the Methods, and the resulting AUC values are provided in Supplementary Table 2. Raw plate-reader data files and accompanying Pipeline Pilot and MATLAB scripts for small-molecule primary screening and low-throughput compound

sensitivity analysis (pertains to Fig. 2, Extended Data Figs. 2a, 3a, 8c, and 10a) are available upon reasonable request. Chromatin profiling data (pertains to Figs. 3, 4, and Extended Data Figs. 4 and 6) are available at GEO (accession number: GSE109794).
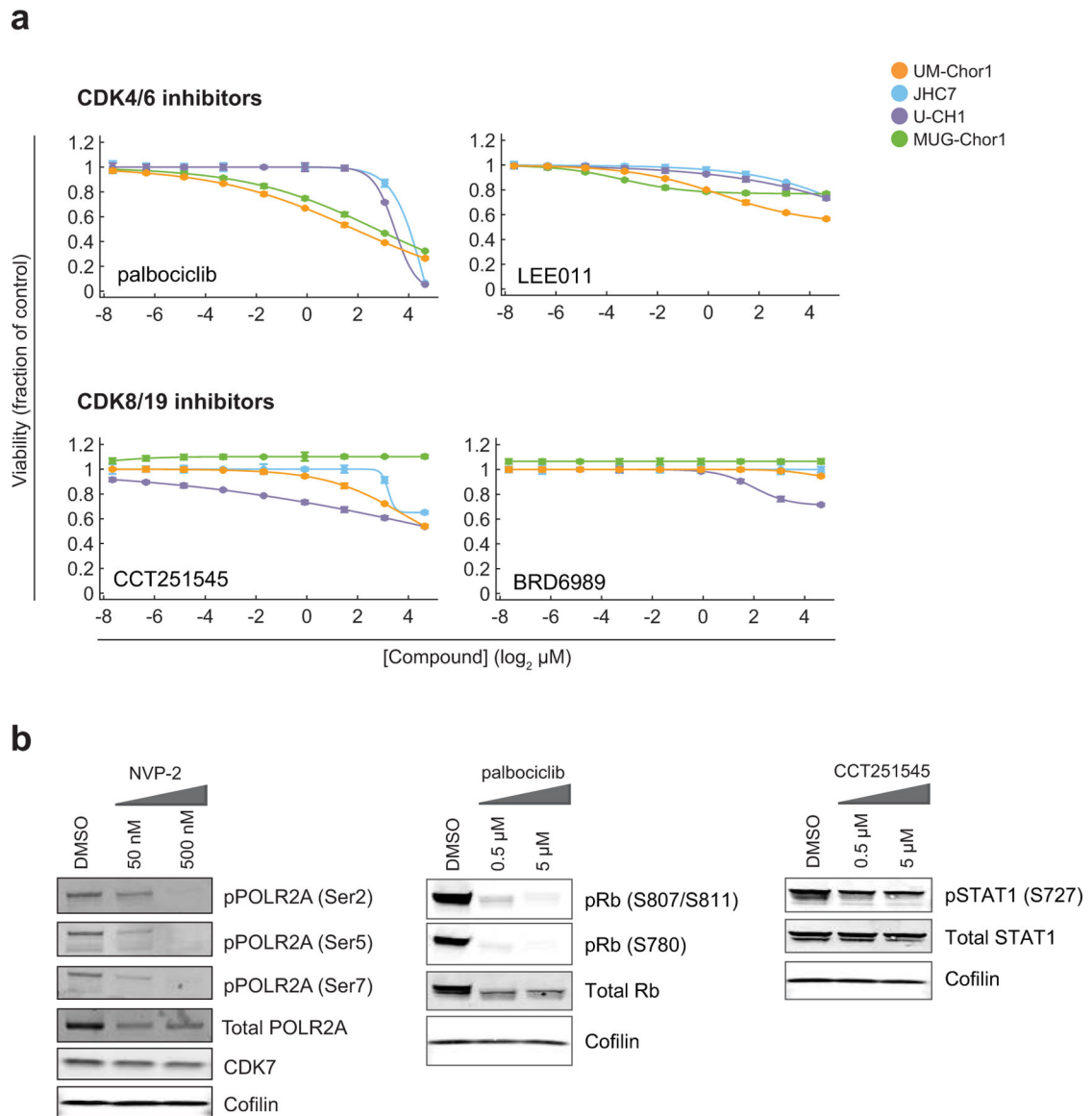
Extended Data
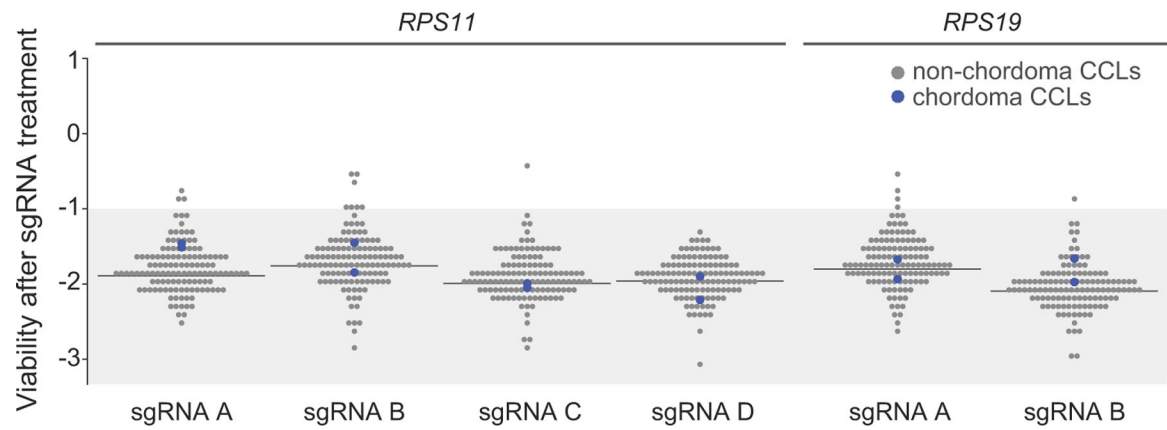
Extended Data Figure 1. Dependency scores for sgRNAs targeting commonly essential genes.
Viability after sgRNA treatment (represented by sgRNA-dependency scores; see Methods)
corresponding to each of the primary screening sgRNAs targeting either *RPS11* or *RPS19*
across 127 cancer cell lines (CCLs), including 2 chordoma CCLs (blue circles). For a given
sgRNA, the median sgRNA-dependency score across 127 cell lines is indicated (gray line).
Lower values indicate greater sgRNA depletion and thus essentiality of the target gene
(shaded region).

a

b
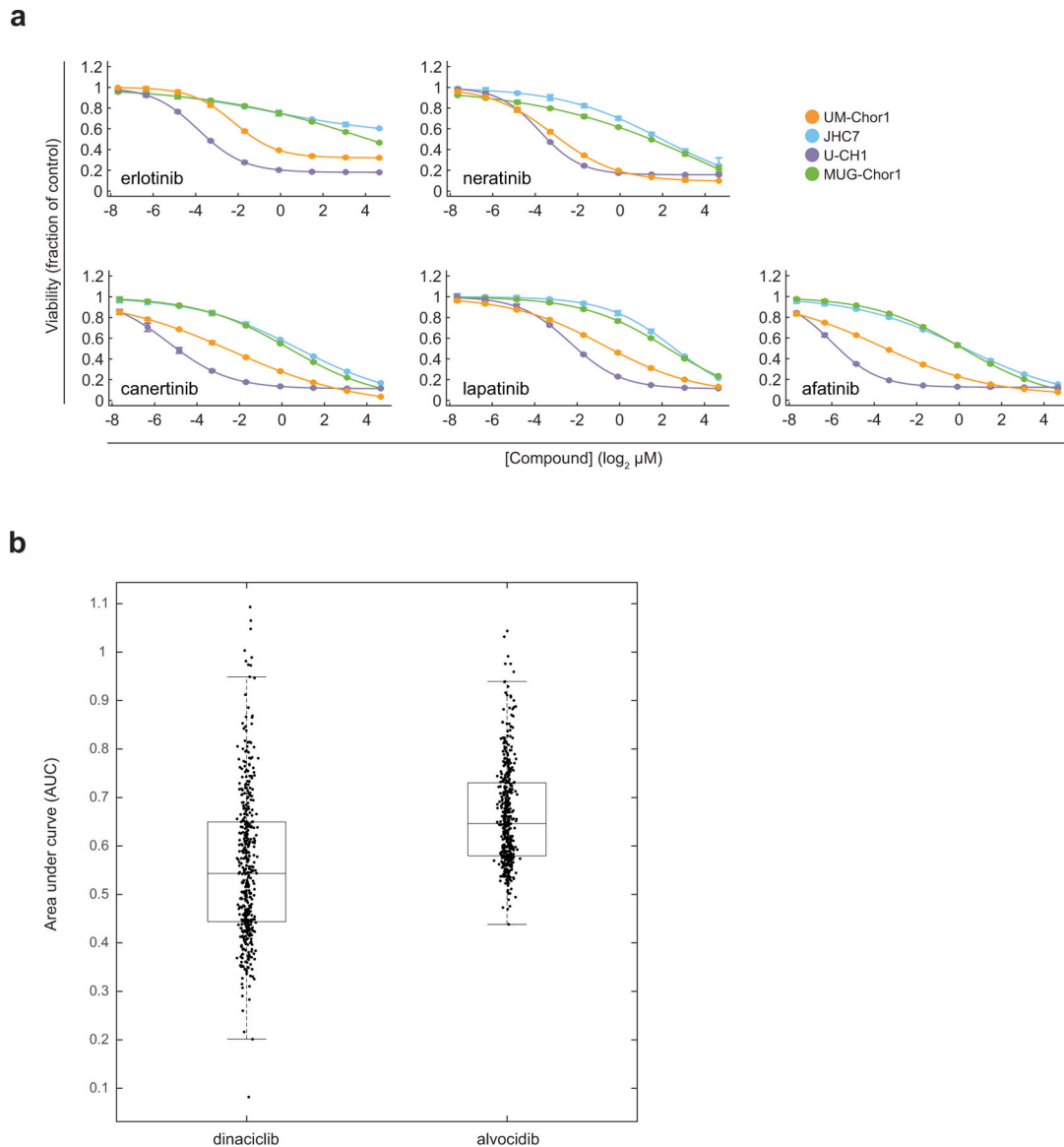
Extended Data Figure 2. Sensitivity of chordoma cells to EGFR and/or ERBB2 inhibitors and of non-chordoma cells to CDK9 inhibitors.

a) Validation of primary screening hit compounds targeting EGFR and/or ERBB2. Four chordoma cell lines were treated with indicated concentrations of candidate antiproliferative compounds and assayed for cell viability after 6 d with CellTiter-Glo. Response data are represented by a fitted curve to the mean fractional viability at each concentration relative to vehicle-treated cells; error bars represent the SEM (n = 4 biological samples measured in parallel). **b)** Dinaciclib and alvocidib have antiproliferative effects across a wide range of cancer cell lines. Area-under-curve (AUC) values corresponding to cell lines in CTRP treated with either dinaciclib or alvocidib. Each point represents a cancer cell line in CTRP treated with the indicated compound. Boxplots depict the inner quartiles (boxes) and median value (horizontal line) with whiskers representing 1.5 × the interquartile range of 445 (dinaciclib-treated) or 440 (alvocidib-treated) cell lines. AUCs were computed as described in the Methods and at https://github.com/remontoire-pac/ctrp-reference/tree/master/auc.

a

b

Extended Data Figure 3. Chordoma cells are less sensitive to CDK4/6 and CDK8/19 inhibitors.
**a)** Response of chordoma cells to compounds targeting CDK4/6 and CDK8/19 proteins. Four chordoma cell lines were treated with indicated concentrations of compounds and assayed for cell viability after 6 d with CellTiter-Glo. Response data are represented by a fitted curve to the mean fractional viability at each concentration relative to vehicle-treated cells; error bars represent the SEM (n = 4 biological samples measured in parallel). **b)** Immunoblot analysis of UM-Chor1 cells treated with indicated concentrations of inhibitors or DMSO for 24 h. The experiment was performed twice for CCT251545 (one representative experiment displayed) and once for other compounds.
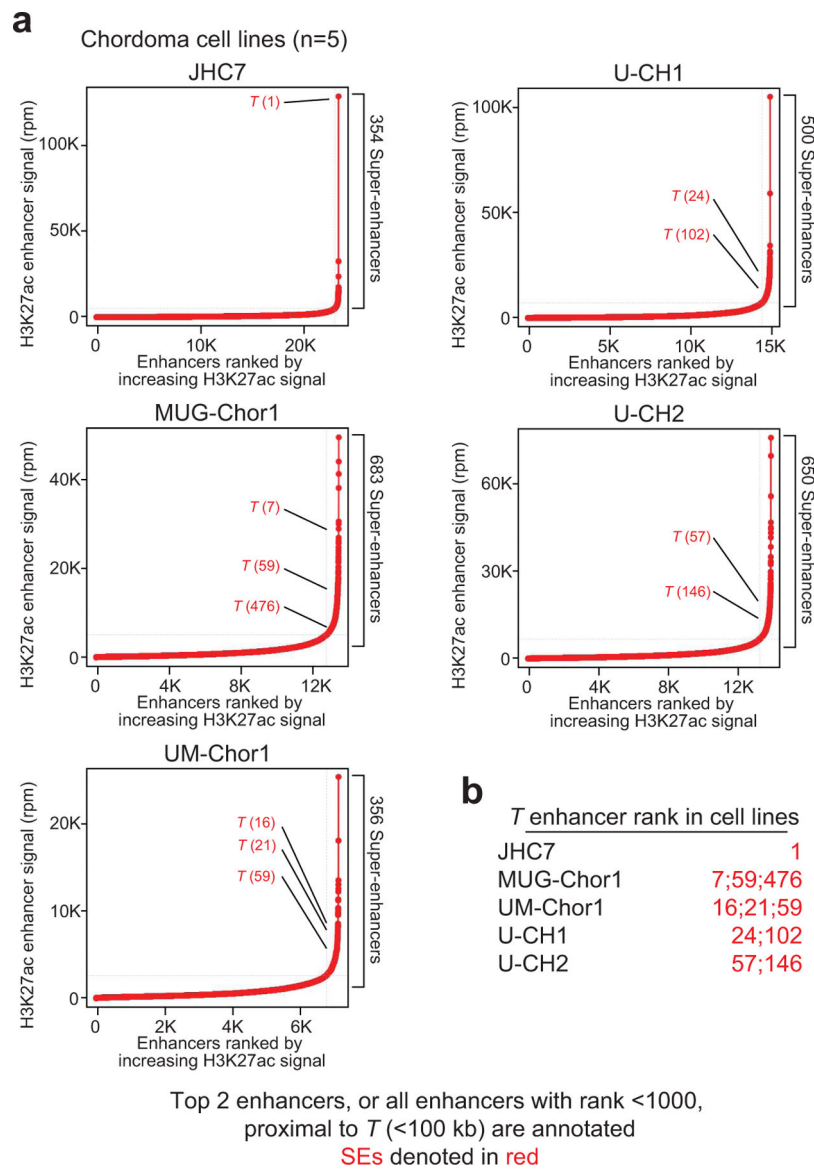
Extended Data Figure 4. *T* **is super-enhancer-associated across chordoma cell lines.**
a) Enhancers in 5 chordoma cell lines ranked by H3K27ac signal in each sample. Enhancers proximal (within 100 kb) to the *T* gene start site are annotated, as described in the figure. Super-enhancers (SEs) were determined by the inflection point of the plot. **b)** Table showing the ranks of top *T*-associated enhancers in each chordoma sample.

a

b

c

SE-associated TFs ranked by expression in chordoma cell lines

115 SE-associated TFs

d
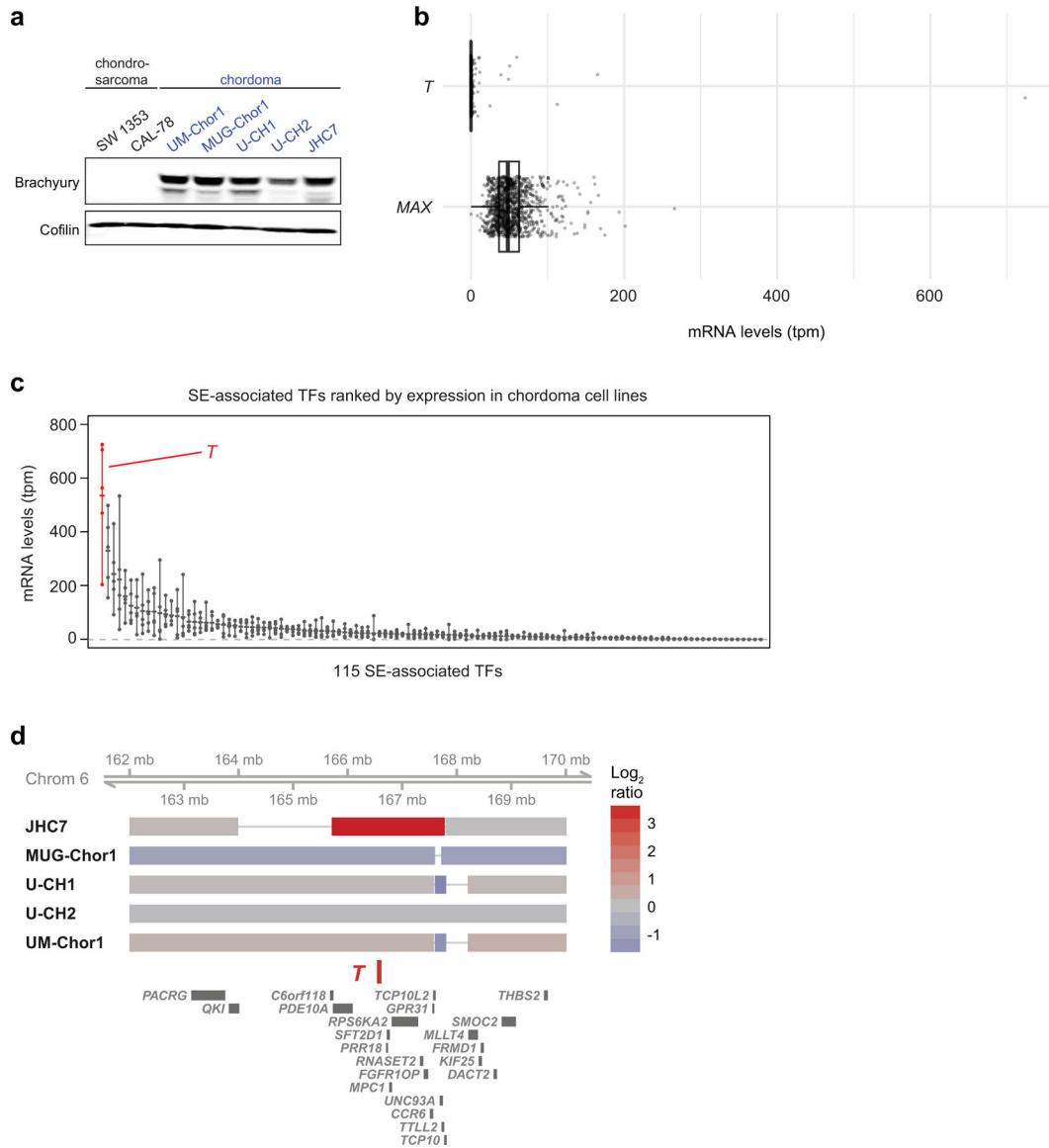
Extended Data Figure 5. Brachyury is highly expressed in chordoma cell lines.
a) Immunoblot analysis of chordoma and chondrosarcoma cell lines. Chordoma cell lines selectively express high levels of the brachyury protein. The experiment was performed once. **b)** Expression of *T* and *MAX*, as measured by RNA-sequencing, across 935 non-chordoma cancer cell lines derived from diverse tumor types. Data were generated as part of the Broad Institute Cancer Cell Line Encyclopedia (quantified data obtained from: https://ocg.cancer.gov/ctd2-data-project/translational-genomics-research-institute-quantified-cancer-cell-line-encyclopedia). Boxplots depict the inner quartiles (boxes) and median value (horizontal line) with whiskers representing 1.5 × the interquartile range. c) Gene expression levels of 115 super-enhancer (SE)-associated transcription factors in 5 chordoma cell lines (points), ranked by mean expression (horizontal ticks). d) *T* is amplified in the JHC7 chordoma cell line. Genomic copy-number alterations, inferred from whole-exome sequencing data, in five chordoma cell lines. A region of 2.06 Mb around the *T* locus on
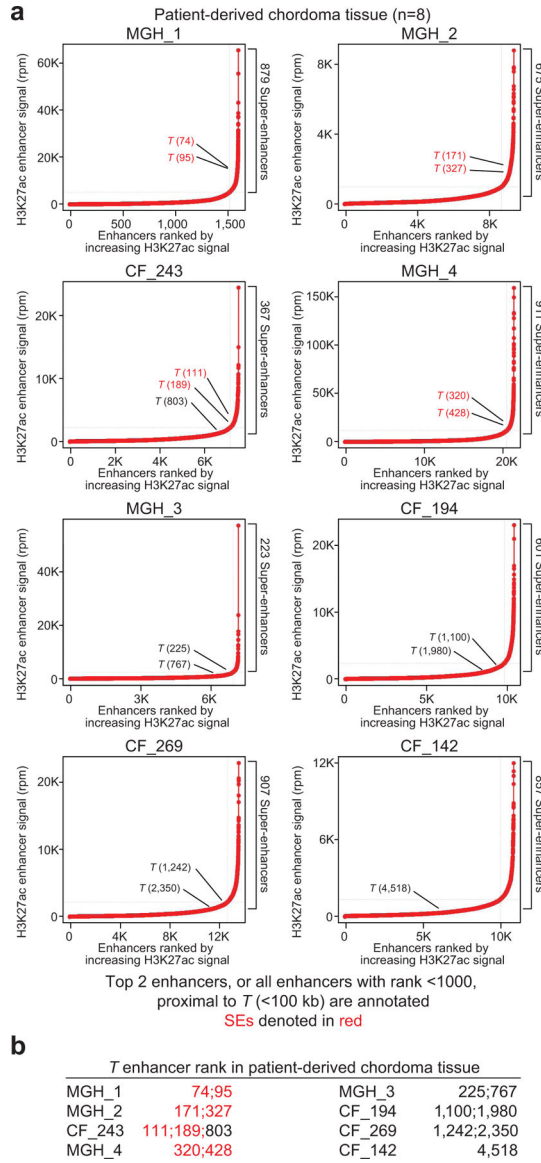
chromosome 6 shows 26-fold amplification in JHC7. This finding is consistent with the 2.6-Mb amplicon inferred from ChIP-seq whole-cell extract.

Extended Data Figure 6. *T* **is super-enhancer-associated in patient-derived chordoma tumors.**
a) Enhancers in chordoma tumors ranked by H3K27ac signal in each sample. Super-enhancers (SEs, red) and typical enhancers (black) proximal (within 100 kb) to the *T* gene start site are annotated. SEs were determined by the inflection point of the plot. **b)** Table showing the ranks of top *T*-associated SEs or typical enhancers in each chordoma sample.

H&E | Brachyury

CF_142

CF_269

CF_194

CF_243
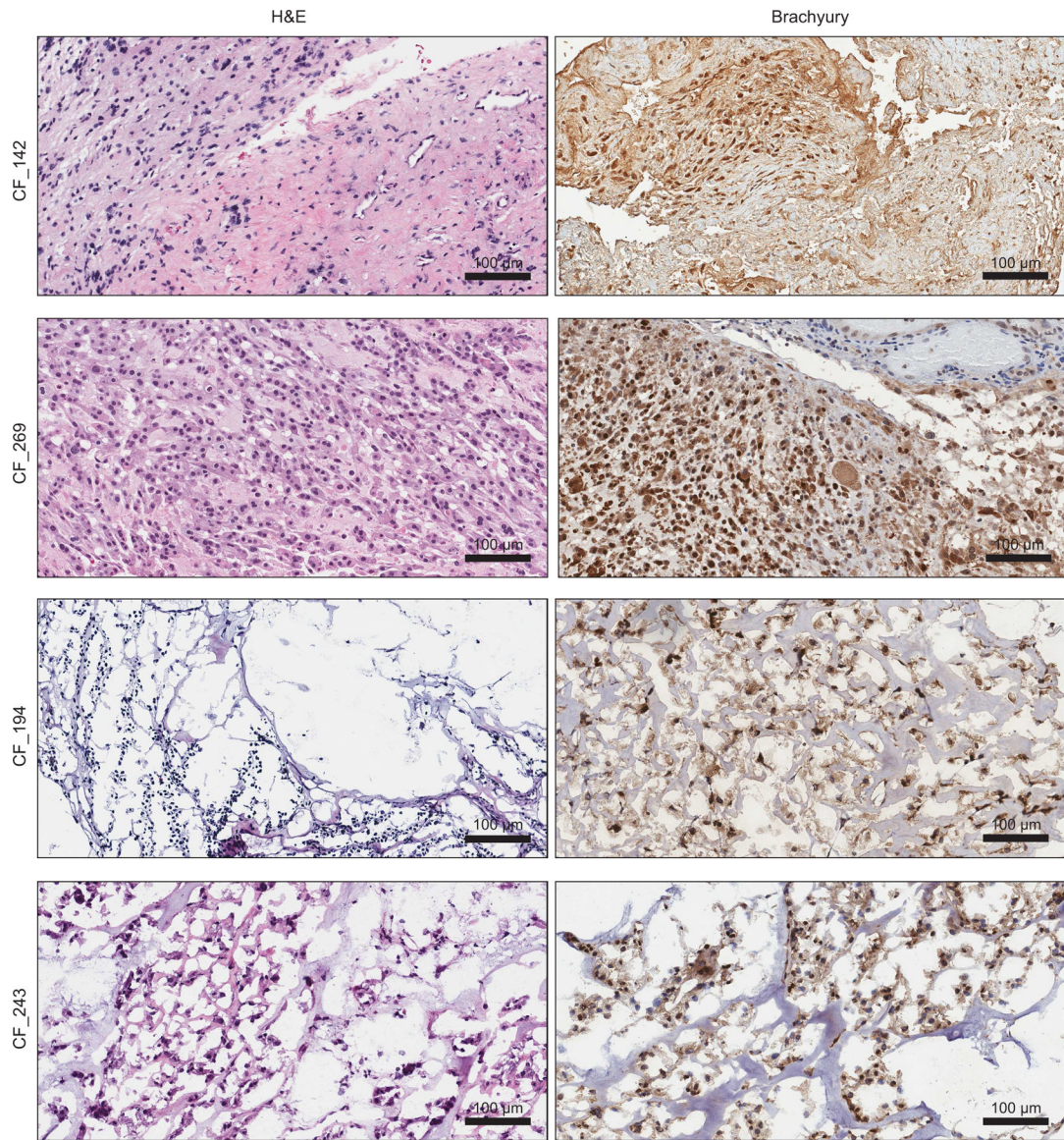
Extended Data Figure 7. Patient-derived chordoma tumors express brachyury.
Immunohistochemical staining of patient-derived chordoma tumors for brachyury
expression. H&E, hematoxylin and eosin. The experiment was performed once.
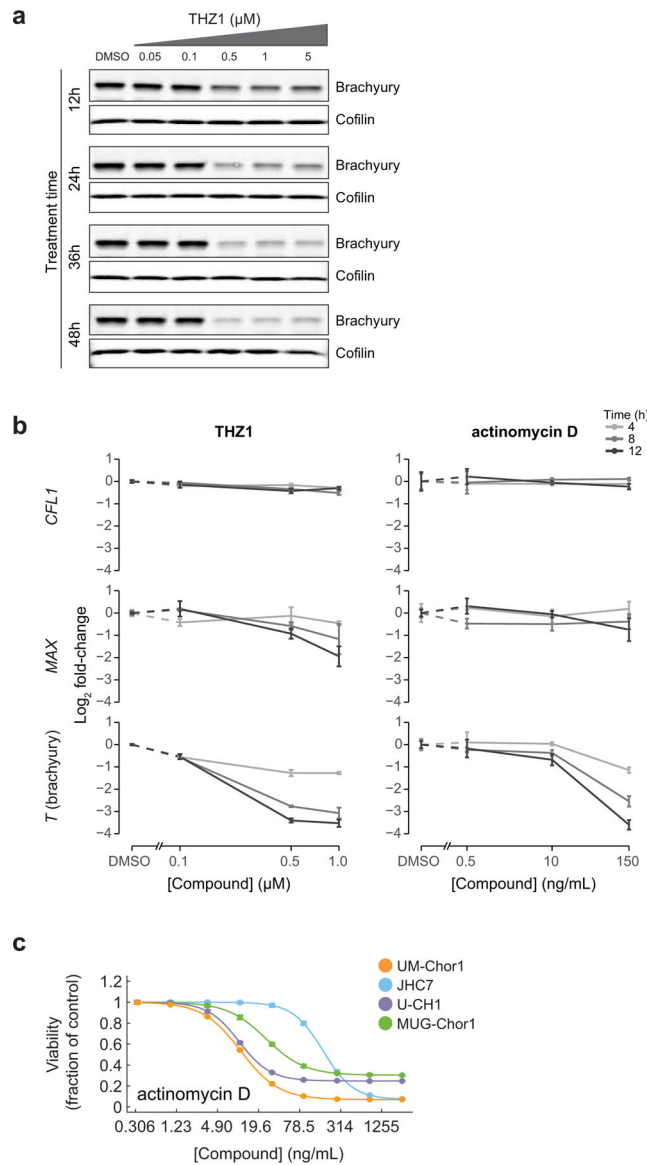
Extended Data Figure 8. THZ1 and actinomycin D reduce expression of *T* (brachyury) in a concentration- and time-dependent fashion.

a) Immunoblot analysis of UM-Chor1 cells treated with indicated concentrations of THZ1 or DMSO for 12, 24, 36, or 48 h. The experiment was performed once. **b**) UM-Chor1 cells were treated with indicated concentrations of compound or DMSO for 4, 8, or 12 h and subjected to RT-qPCR. Data are expressed as the $\log_2$ fold-change of transcript levels relative to vehicle-treated cells, normalized to *GAPDH* levels, and represent the mean ± SD (n = 3 biological samples measured in parallel). Results of statistical analyses of RT-qPCR data, derived from a one-sided Welch's t-test, are reported in Supplementary Table 9. **c**) Response of chordoma cells to treatment with actinomycin D. Four chordoma cell lines were treated with indicated concentrations of compound and assayed for cell viability after 6 d with CellTiter-Glo. Response data are represented by a fitted curve to the mean fractional viability at each concentration relative to vehicle-treated cells; error bars represent the SEM (n = 4 biological samples measured in parallel).
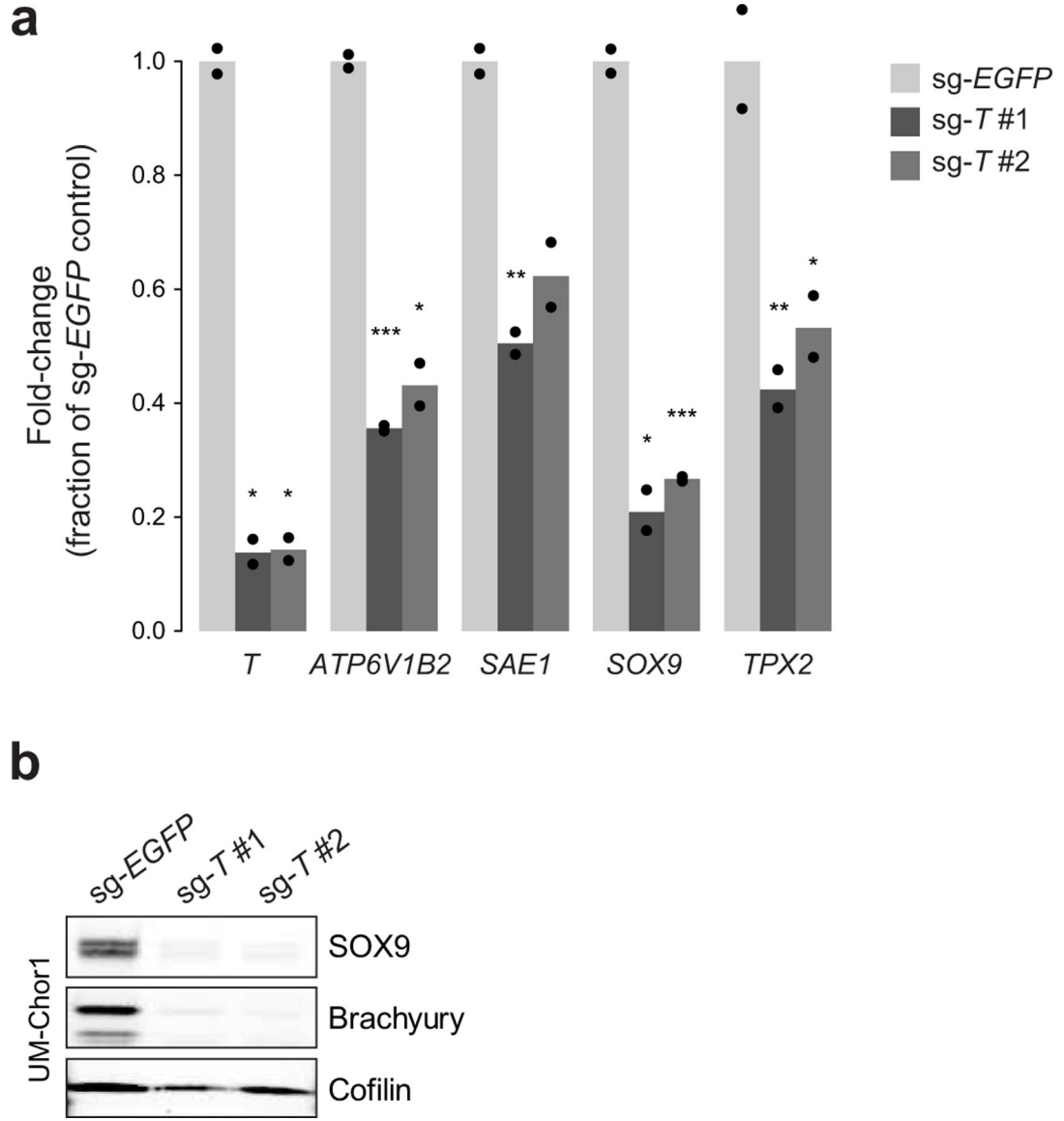
Extended Data Figure 9. Expression of *ATP6V1B2*, *SAE1*, *SOX9*, and *TPX2* is downregulated following sgRNA-mediated *T* (brachyury) repression.

a) UM-Chor1 cells were transduced with sgRNAs targeting *T* or a non-targeting sgRNA control and subjected to RT-qPCR. Data are expressed as the fold-change of transcript levels relative to sgRNA control-treated cells, normalized to *GAPDH* levels, and represent the mean (n = 2 biological samples measured in parallel, represented by black points). * $p < 0.05$; ** $p < 0.01$; *** $p < 0.001$; p-values were derived from a one-sided Welch's t-test. Exact p-values and effects sizes are reported in Supplementary Table 9. **b)** Immunoblot analysis of UM-Chor1 cells transduced with sgRNAs targeting *T* or a non-targeting sgRNA control. SgRNA treatment was performed once and immunoblotting was performed twice (one representative experiment displayed).
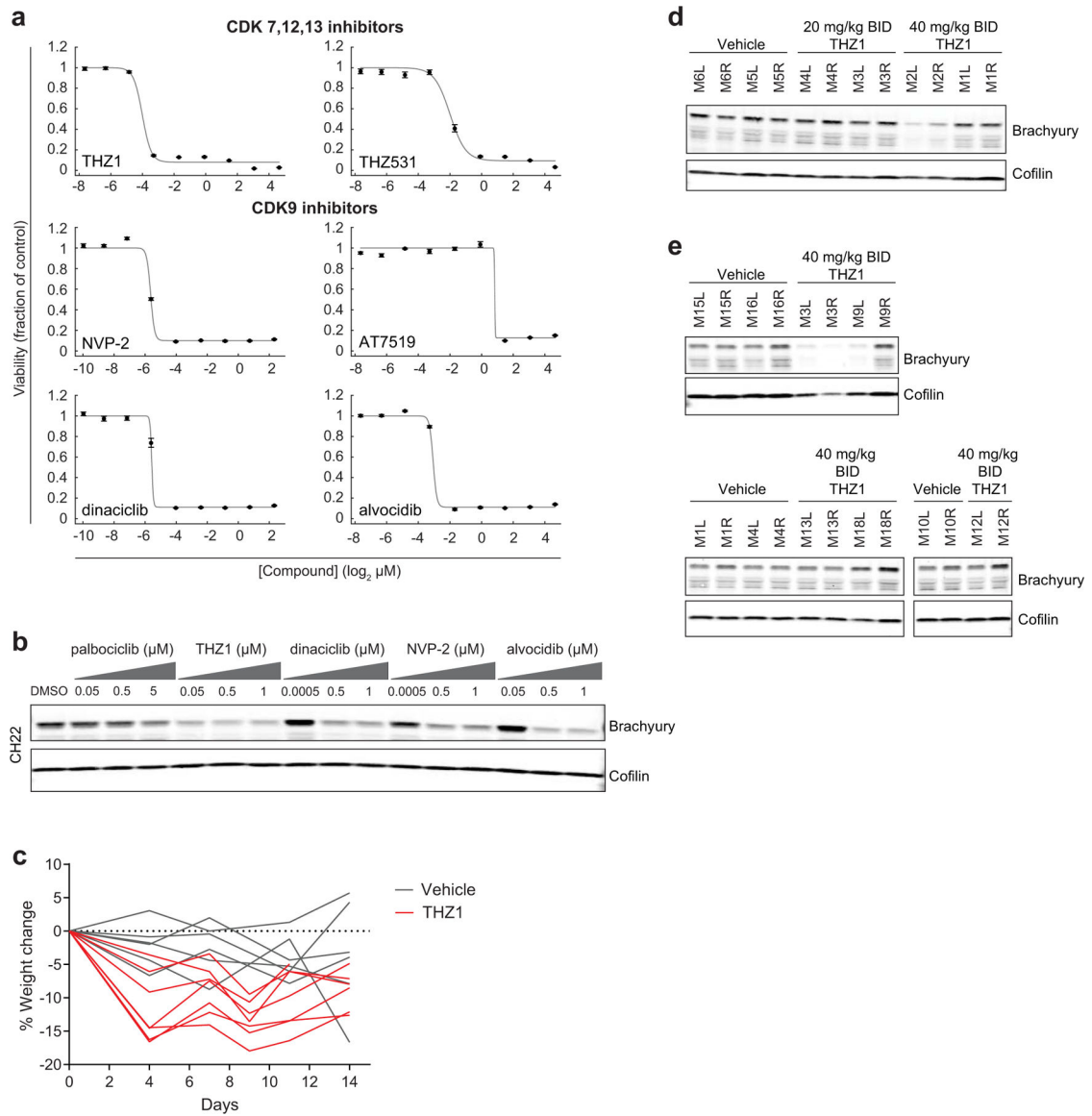
Extended Data Figure 10. THZ1 treatment can reduce brachyury expression in CH22 cells *ex vivo* and *in vivo*.

a) CH22 chordoma cells were treated with indicated concentrations of transcriptional CDK inhibitors and assayed for cell viability after 6 d with CellTiter-Glo. Response data are represented by a fitted curve to the mean fractional viability at each concentration relative to vehicle-treated cells; error bars represent the SEM (n = 4 biological samples measured in parallel). **b)** Immunoblot analysis of CH22 cells treated with indicated concentrations of inhibitors targeting CDK4/6 (palbociclib), CDK7/12/13 (THZ1), or CDK9 (dinaciclib, NVP-2, alvocidib) or DMSO for 48 h. The experiment was performed once. **c)** Weight change of mice treated with THZ1 or vehicle for the study depicted in Fig. 4h–i. d) THZ1 can downregulate brachyury expression *in vivo*. Immunoblot analysis of CH22 xenograft tumors following treatment with indicated doses of THZ1 or vehicle twice daily for 5 d. The experiment was performed once. **e)** Immunoblot analysis of CH22 xenograft tumors following treatment with THZ1 or vehicle twice daily for 3 d. Top and bottom panels

represent two independent studies (bottom panel corresponds to the study depicted in Fig. 4h–i).

Supplementary Material

Refer to Web version on PubMed Central for supplementary material.

ACKNOWLEDGEMENTS

REFERENCES

1. Stacchiotti S, Sommer J & Chordoma Global Consensus Group. Building a global consensus approach to chordoma: a position paper from the medical and patient community. Lancet Oncol 16, e71–83 (2015). [PubMed: 25638683]

2. Choy E, et al. Genotyping cancer-associated genes in chordoma identifies mutations in oncogenes and areas of chromosomal loss involving CDKN2A, PTEN, and SMARCB1. PLoS One 9, e101283 (2014). [PubMed: 24983247]

3. Tarpey PS, et al. The driver landscape of sporadic chordoma. Nature communications 8, 890 (2017).

4. Kwiatkowski N, et al. Targeting transcription regulation in cancer with a covalent CDK7 inhibitor. Nature 511, 616–620 (2014). [PubMed: 25043025]

5. Bradner JE, Hnisz D & Young RA Transcriptional Addiction in Cancer. Cell 168, 629–643 (2017). [PubMed: 28187285]

6. McMaster ML, Goldstein AM, Bromley CM, Ishibe N & Parry DM Chordoma: incidence and survival patterns in the United States, 1973–1995. Cancer causes & control : CCC 12, 1–11 (2001). [PubMed: 11227920]

7. Barry JJ, et al. The next step: innovative molecular targeted therapies for treatment of intracranial chordoma patients. Neurosurgery 68, 231–240; discussion 240–231 (2011). [PubMed: 21099719]

8. Salisbury JR The pathology of the human notochord. The Journal of pathology 171, 253–255 (1993). [PubMed: 8158454]

9. Vujovic S, et al. Brachyury, a crucial regulator of notochordal development, is a novel biomarker for chordomas. The Journal of pathology 209, 157–165 (2006). [PubMed: 16538613]

10. Showell C, Binder O & Conlon FL T-box genes in early embryogenesis. Developmental dynamics : an official publication of the American Association of Anatomists 229, 201–218 (2004). [PubMed: 14699590]

11. Yang XR, et al. T (brachyury) gene duplication confers major susceptibility to familial chordoma. Nat Genet 41, 1176–1178 (2009). [PubMed: 19801981]

12. Pillay N, et al. A common single-nucleotide variant in T is strongly associated with chordoma. Nat Genet 44, 1185–1187 (2012). [PubMed: 23064415]

13. Presneau N, et al. Role of the transcription factor T (brachyury) in the pathogenesis of sporadic chordoma: a genetic and functional-based study. The Journal of pathology 223, 327–335 (2011). [PubMed: 21171078]

14. Hsu W, et al. Generation of chordoma cell line JHC7 and the identification of Brachyury as a novel molecular target. Journal of neurosurgery 115, 760–769 (2011). [PubMed: 21699479]

15. Shah SR, et al. Brachyury-YAP Regulatory Axis Drives Stemness and Growth in Cancer. Cell reports 21, 495–507 (2017). [PubMed: 29020634]

16. Palena C, et al. The human T-box mesodermal transcription factor Brachyury is a candidate target for T-cell-mediated cancer immunotherapy. Clin Cancer Res 13, 2471–2478 (2007). [PubMed: 17438107]

17. Garraway LA & Sellers WR Lineage dependency and lineage-survival oncogenes in human cancer. Nat Rev Cancer 6, 593–602 (2006). [PubMed: 16862190]

18. Berg T Inhibition of transcription factors with small organic molecules. Current opinion in chemical biology 12, 464–471 (2008). [PubMed: 18706517]

19. Sharifnia T, Hong AL, Painter CA & Boehm JS Emerging Opportunities for Target Discovery in Rare Cancers. Cell chemical biology 24, 1075–1091 (2017). [PubMed: 28938087]

20. Meyers RM, et al. Computational correction of copy number effect improves specificity of CRISPR-Cas9 essentiality screens in cancer cells. Nat Genet (2017).

21. Barrionuevo F, Taketo MM, Scherer G & Kispert A Sox9 is required for notochord maintenance in mice. Developmental biology 295, 128–140 (2006). [PubMed: 16678811]

22. Seashore-Ludlow B, et al. Harnessing Connectivity in a Large-Scale Small-Molecule Sensitivity Dataset. Cancer Discov 5, 1210–1223 (2015). [PubMed: 26482930]

23. Whittaker SR, Mallinger A, Workman P & Clarke PA Inhibitors of cyclin-dependent kinases as cancer therapeutics. Pharmacology & therapeutics 173, 83–105 (2017). [PubMed: 28174091]

24. Zhang T, et al. Covalent targeting of remote cysteine residues to develop CDK12 and CDK13 inhibitors. Nat Chem Biol 12, 876–884 (2016). [PubMed: 27571479]

25. Galli GG, et al. YAP Drives Growth by Controlling Transcriptional Pause Release from Dynamic Enhancers. Mol Cell 60, 328–337 (2015). [PubMed: 26439301]

26. Modjtahedi H, Cho BC, Michel MC & Solca F A comprehensive review of the preclinical efficacy profile of the ErbB family blocker afatinib in cancer. Naunyn-Schmiedeberg's archives of pharmacology 387, 505–521 (2014).

27. Scheipl S, et al. EGFR inhibitors identified as a potential treatment for chordoma in a focused compound screen. The Journal of pathology 239, 320–334 (2016). [PubMed: 27102572]

28. Tripathy D, Bardia A & Sellers WR Ribociclib (LEE011): Mechanism of Action and Clinical Impact of This Selective Cyclin-Dependent Kinase 4/6 Inhibitor in Various Solid Tumors. Clin Cancer Res 23, 3251–3262 (2017). [PubMed: 28351928]

29. Dale T, et al. A selective chemical probe for exploring the role of CDK8 and CDK19 in human disease. Nat Chem Biol 11, 973–980 (2015). [PubMed: 26502155]

30. Johannessen L, et al. Small-molecule studies identify CDK8 as a regulator of IL-10 in myeloid cells. Nat Chem Biol (2017).

31. Loven J, et al. Selective inhibition of tumor oncogenes by disruption of super-enhancers. Cell 153, 320–334 (2013). [PubMed: 23582323]

32. Hnisz D, et al. Super-enhancers in the control of cell identity and disease. Cell 155, 934–947 (2013). [PubMed: 24119843]

33. Nelson AC, et al. An integrated functional genomics approach identifies the regulatory network directed by brachyury (T) in chordoma. The Journal of pathology 228, 274–285 (2012). [PubMed: 22847733]

34. Buenrostro JD, Giresi PG, Zaba LC, Chang HY & Greenleaf WJ Transposition of native chromatin for fast and sensitive epigenomic profiling of open chromatin, DNA-binding proteins and nucleosome position. Nat Methods 10, 1213–1218 (2013). [PubMed: 24097267]

35. Lin CY, et al. Active medulloblastoma enhancers reveal subgroup-specific cellular origins. Nature 530, 57–62 (2016). [PubMed: 26814967]

36. Schwab JH, et al. Chordoma and chondrosarcoma gene profile: implications for immunotherapy. Cancer immunology, immunotherapy : CII 58, 339–349 (2009). [PubMed: 18641983]

37. Jager D, et al. HOXA7, HOXA9, and HOXA10 are differentially expressed in clival and sacral chordomas. Scientific reports 7, 2032 (2017). [PubMed: 28515451]

38. Shalaby A, et al. The role of epidermal growth factor receptor in chordoma pathogenesis: a potential therapeutic target. The Journal of pathology 223, 336–346 (2011). [PubMed: 21171079]

39. Trask DK & Muller MT Stabilization of type I topoisomerase-DNA covalent complexes by actinomycin D. Proc Natl Acad Sci U S A 85, 1417–1421 (1988). [PubMed: 2830618]

40. Liu X, et al. Establishment and characterization of a novel chordoma cell line: CH22. Journal of orthopaedic research : official publication of the Orthopaedic Research Society 30, 1666–1673 (2012). [PubMed: 22504929]

41. Barretina J, et al. The Cancer Cell Line Encyclopedia enables predictive modelling of anticancer drug sensitivity. Nature 483, 603–607 (2012). [PubMed: 22460905]

42. Doench JG, et al. Rational design of highly active sgRNAs for CRISPR-Cas9-mediated gene inactivation. Nat Biotechnol 32, 1262–1267 (2014). [PubMed: 25184501]

43. Cowley GS, et al. Parallel genome-scale loss of function screens in 216 cancer cell lines for the identification of context-specific genetic dependencies. Scientific data 1, 140035 (2014). [PubMed: 25984343]

44. Aguirre AJ, et al. Genomic Copy Number Dictates a Gene-Independent Cell Response to CRISPR/ Cas9 Targeting. Cancer Discov 6, 914–929 (2016). [PubMed: 27260156]

45. Johnson WE, Li C & Rabinovic A Adjusting batch effects in microarray expression data using empirical Bayes methods. Biostatistics 8, 118–127 (2007). [PubMed: 16632515]

46. Shalem O, et al. Genome-scale CRISPR-Cas9 knockout screening in human cells. Science 343, 84–87 (2014). [PubMed: 24336571]

47. Dancik V, et al. Connecting Small Molecules with Similar Assay Performance Profiles Leads to New Biological Hypotheses. Journal of biomolecular screening 19, 771–781 (2014). [PubMed: 24464433]

48. Dobin A, et al. STAR: ultrafast universal RNA-seq aligner. Bioinformatics 29, 15–21 (2013). [PubMed: 23104886]

49. Love MI, Huber W & Anders S Moderated estimation of fold change and dispersion for RNA-seq data with DESeq2. Genome Biol 15, 550 (2014). [PubMed: 25516281]

50. Subramanian A, et al. Gene set enrichment analysis: a knowledge-based approach for interpreting genome-wide expression profiles. Proc Natl Acad Sci U S A 102, 15545–15550 (2005). [PubMed: 16199517]

51. Mootha VK, et al. PGC-1alpha-responsive genes involved in oxidative phosphorylation are coordinately downregulated in human diabetes. Nat Genet 34, 267–273 (2003). [PubMed: 12808457]

52. Van der Auwera GA, et al. From FastQ data to high confidence variant calls: the Genome Analysis Toolkit best practices pipeline. Current protocols in bioinformatics 43, 11–33 (2013). [PubMed: 25431634]

53. Li H & Durbin R Fast and accurate short read alignment with Burrows-Wheeler transform. Bioinformatics 25, 1754–1760 (2009). [PubMed: 19451168]

54. McKenna A, et al. The Genome Analysis Toolkit: a MapReduce framework for analyzing next-generation DNA sequencing data. Genome Res 20, 1297–1303 (2010). [PubMed: 20644199]

55. Langmead B & Salzberg SL Fast gapped-read alignment with Bowtie 2. Nat Methods 9, 357–359 (2012). [PubMed: 22388286]

56. Zhang Y, et al. Model-based analysis of ChIP-Seq (MACS). Genome Biol 9, R137 (2008). [PubMed: 18798982]

57. Brown JD, et al. NF-κB Directs Dynamic Super Enhancer Formation in Inflammation and Atherogenesis. Molecular cell 56, 219–231 (2014). [PubMed: 25263595]

58. Johannessen CM, et al. COT drives resistance to RAF inhibition through MAP kinase pathway reactivation. Nature 468, 968–972 (2010). [PubMed: 21107320]
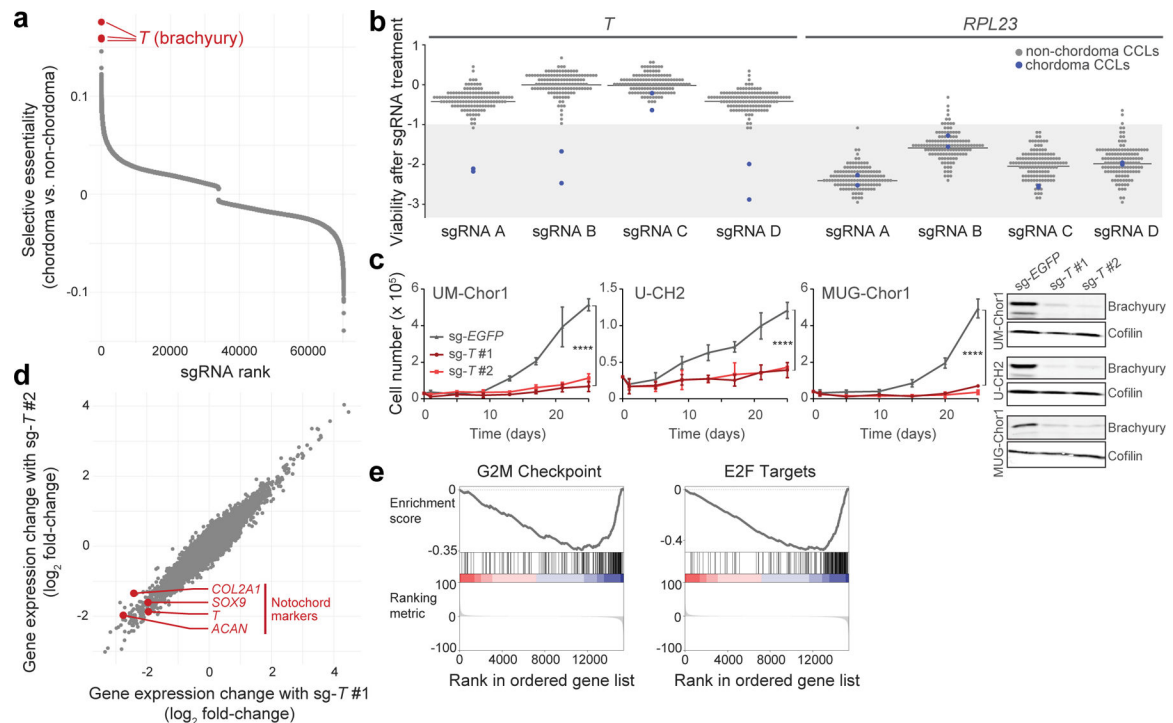
59. Quinlan AR & Hall IM BEDTools: a flexible suite of utilities for comparing genomic features. Bioinformatics 26, 841–842 (2010). [PubMed: 20110278]

60. Heinz S, et al. Simple combinations of lineage-determining transcription factors prime cis-regulatory elements required for macrophage and B cell identities. Mol Cell 38, 576–589 (2010). [PubMed: 20513432]

Figure 1. Genome-scale CRISPR-Cas9 screening identifies *T* (brachyury) as a selectively essential gene in chordoma cells.
a) Comparative analysis of genome-scale CRISPR-Cas9 screening results generated in UM-Chor1 and MUG-Chor1 chordoma cell lines versus 125 non-chordoma cancer cell lines. SgRNAs were ranked by and plotted against selectively lethal effects (RNMI scores; see Methods) in chordoma versus non-chordoma cell lines. The top three sgRNAs (red circles) all target *T*. **b)** Viability after sgRNA treatment (represented by sgRNA-dependency scores; see Methods) corresponding to each of the four primary screening sgRNAs targeting either *T* or *RPL23* across 127 cancer cell lines (CCLs), including 2 chordoma CCLs (blue circles). For each sgRNA, the median sgRNA-dependency score across 127 cell lines is indicated (gray line). Lower values indicate greater sgRNA depletion and thus essentiality of the target gene (shaded region). **c)** (Left) Proliferation of chordoma cell lines transduced with sgRNAs targeting *T* or a non-targeting sgRNA control. Points represent the mean ± SD (n = 3 biological samples measured in parallel). **** $p < 0.0001$, derived from a two-way ANOVA (p-values for the test comparing sg-*EGFP* and sg-*T*#1 are displayed). Exact p-values and effect sizes are reported in Supplementary Table 9. (Right) Immunoblot analysis of transduced cells confirming sgRNA-mediated protein repression. Proliferation experiments were performed twice with UM-Chor1 and U-CH2 cells (one representative experiment displayed for each) and once with MUG-Chor1 cells; immunoblots were performed once. **d)** Relative gene expression of UM-Chor1 cells transduced with one of two sgRNAs targeting *T* versus a non-targeting sgRNA control. Gene expression was measured with RNA sequencing. Data represent two biological replicates per condition. **e)** Gene-set enrichment analysis results show significant downregulation of genes associated with cell cycle progression, such as drivers of G2/M checkpoint progression and E2F targets.
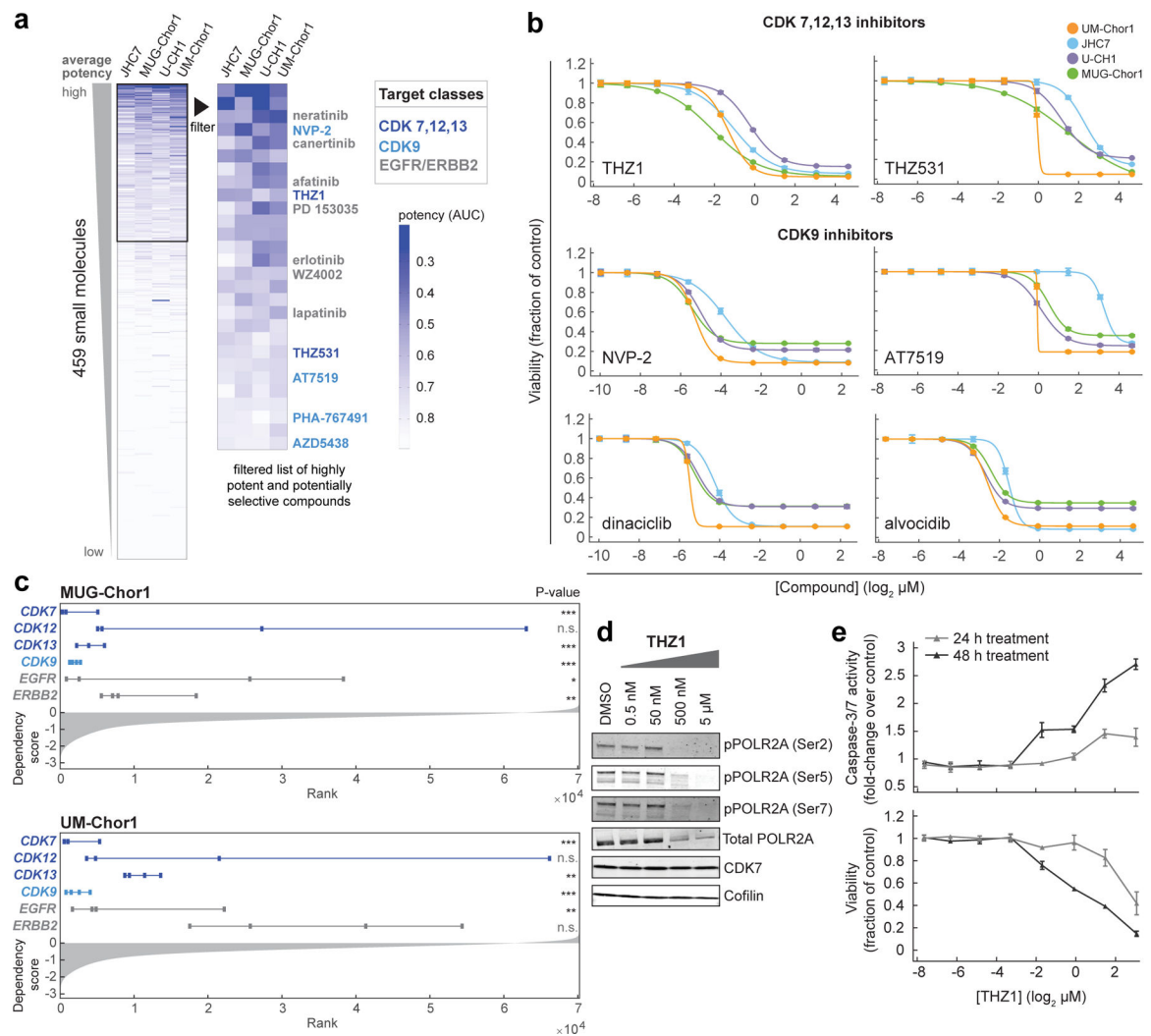
Figure 2. Small-molecule sensitivity profiling identifies inhibitors of CDK7/12/13 and CDK9 as potent antiproliferative agents in chordoma cells.

a) Profiling results for 459 small molecules tested in four chordoma cell lines. Data represent area-under-curve (AUC) values calculated from 8-point concentration-response curves generated in duplicate, and coloring in the heatmap is representative of smaller AUC values (blue) corresponding to more potent effects (AUC value of 1 = vehicle control; value of 0 = complete killing at all concentrations). Left heatmap, all compounds were ranked by average potency in chordoma cell lines; potent compounds (average AUC < 0.8, boxed) were then filtered to exclude those with cytotoxic effects non-selective for chordoma cell lines versus up to 891 non-chordoma cancer cell lines, when such data were available in CTRP. Compounds that were only tested in chordoma cell lines and were not available in CTRP were not filtered beyond the initial potency filter. Twenty-eight compounds (right heatmap) passed these criteria. **b)** Validation of primary screening hits and related compounds. Four chordoma cell lines were treated with indicated concentrations of candidate antiproliferative compounds and assayed for cell viability after 6 d with CellTiter-Glo. Response data are represented by a fitted curve to the mean fractional viability at each concentration relative to vehicle-treated cells; error bars represent the SEM (n = 4 biological

samples measured in parallel). **c)** Rankings of sgRNA-level dependency scores (see Methods) for the indicated genes following genome-scale CRISPR-Cas9 screening (see Fig. 1). Points represent each of four sgRNAs targeting a given gene that were present in the pooled CRISPR library used for screening. P-values were derived from a one-sided Mann-Whitney test. *, $p < 0.05$; **, $p < 0.01$; *** $p < 0.001$; n.s., not significant. The gray waterfall plot represents ranked dependency scores for all sgRNAs tested (median dependency score = −0.3257 for MUG-Chor1; median = −0.3283 for UM-Chor1). Median dependency scores for the four sgRNAs and exact Mann-Whitney p-values corresponding to each gene are reported in Supplementary Table 9. **d)** Immunoblot analysis of UM-Chor1 cells treated with indicated concentrations of THZ1 or DMSO for 24 h. Data are representative of two independent experiments. **e)** Caspase-3/7 activity (top) and cell viability (bottom) following THZ1 treatment of UM-Chor1 cells. Caspase-3/7 activity and cell viability were measured in parallel at the indicated time points using Caspase-Glo 3/7 and CellTiter-Glo reagents, respectively. Data are expressed as the fold-change of caspase-3/7 activity (top) or fraction of cell viability (bottom) relative to vehicle-treated cells and represent the mean ± SD (n = 4 biological samples measured in parallel).
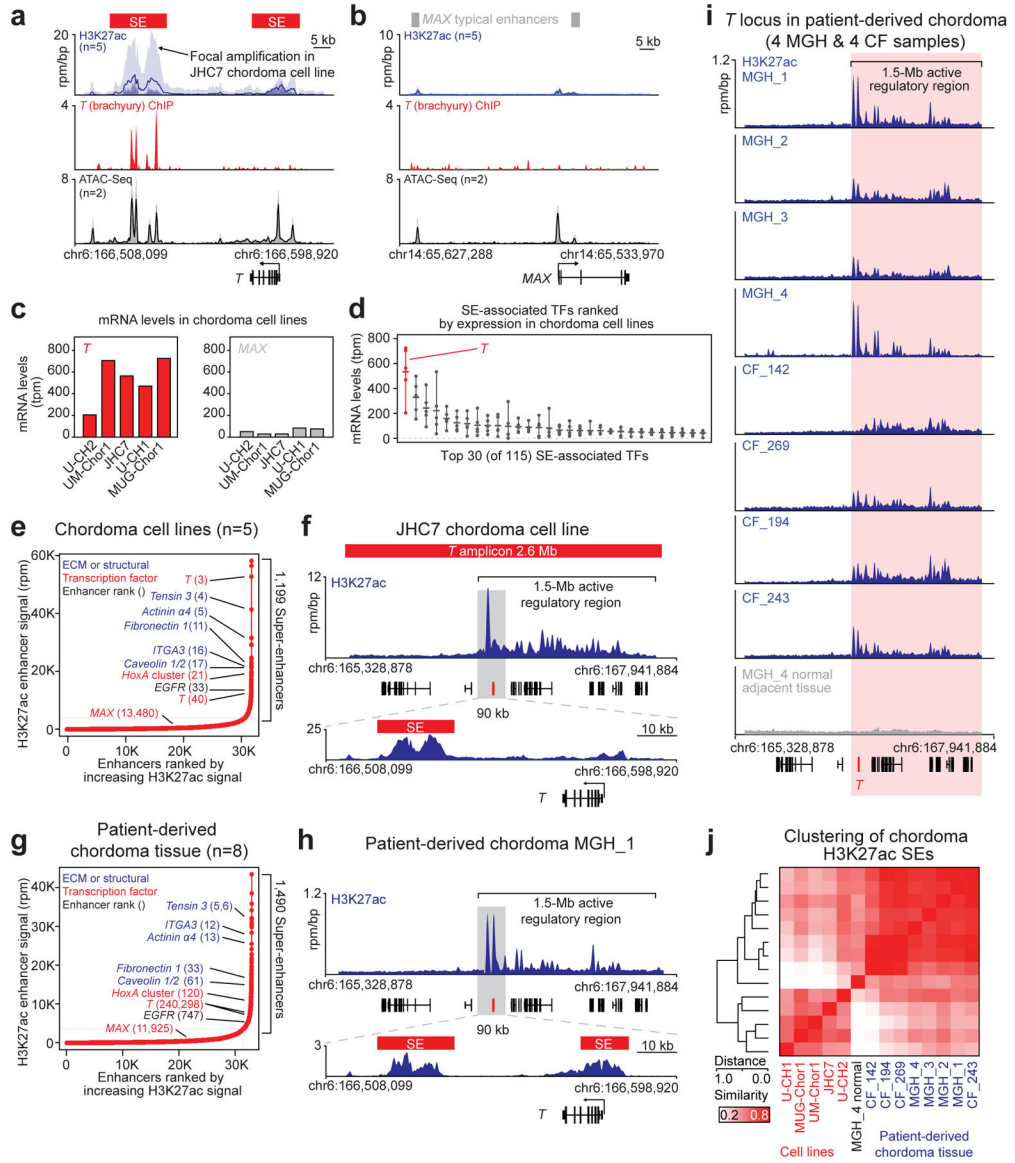
Figure 3. *T* (brachyury) is super-enhancer-associated and highly active across chordoma cell lines and in patient-derived chordoma tumors.

a,b) Gene tracks of H3K27ac, brachyury, and ATAC-seq signal (units of reads per million per base pair) at the *T* and *MAX* gene loci. For datasets with multiple samples (H3K27ac and ATAC-seq), signals for samples are plotted as a translucent shape and darker regions indicate regions with signal in more samples. An opaque line is plotted and gives the average signal across all samples in the group. H3K27Ac ChIP-seq was performed on 5 chordoma cell lines (UM-Chor1, MUG-Chor1, U-CH2, U-CH1, JHC7); brachyury ChIP-seq was performed on 1 chordoma cell line (U-CH1) as previously reported[33]; and ATAC-seq was performed on two chordoma cell lines (2 biological replicates for U-CH2 and 1 replicate for MUG-Chor1). **c)** Bar graphs of RNA-seq mRNA levels for *T* and *MAX* across 5 chordoma cell lines. Units are in transcripts per million (tpm). **d)** Gene expression levels of the top 30 (of 115) super-enhancer (SE)-associated transcription factors in 5 chordoma cell lines (points), ranked by mean expression (horizontal ticks). **e,g)** Enhancers in chordoma cell lines

(UM-Chor1, MUG-Chor1, U-CH2, U-CH1, JHC7) or patient-derived chordoma tumor tissue ranked by average H3K27ac signal across samples. SEs and associated genes are annotated along the vertical axis and were determined by the inflection point of the plot. **f,h)** Gene tracks of H3K27ac signal at the *T*-amplified region in the JCH7 cell line and the corresponding region in the MGH_1 chordoma tumor. The amplicon and *T*-proximal SEs are shown (red boxes). **i)** Gene tracks of H3K27ac signal across eight patient-derived chordoma tumor samples and one matched normal adjacent muscle sample at the *T* locus. **j)** Clustergram of chordoma samples hierarchically clustered by similarity of H3K27ac signal at the union of all SE regions across samples.
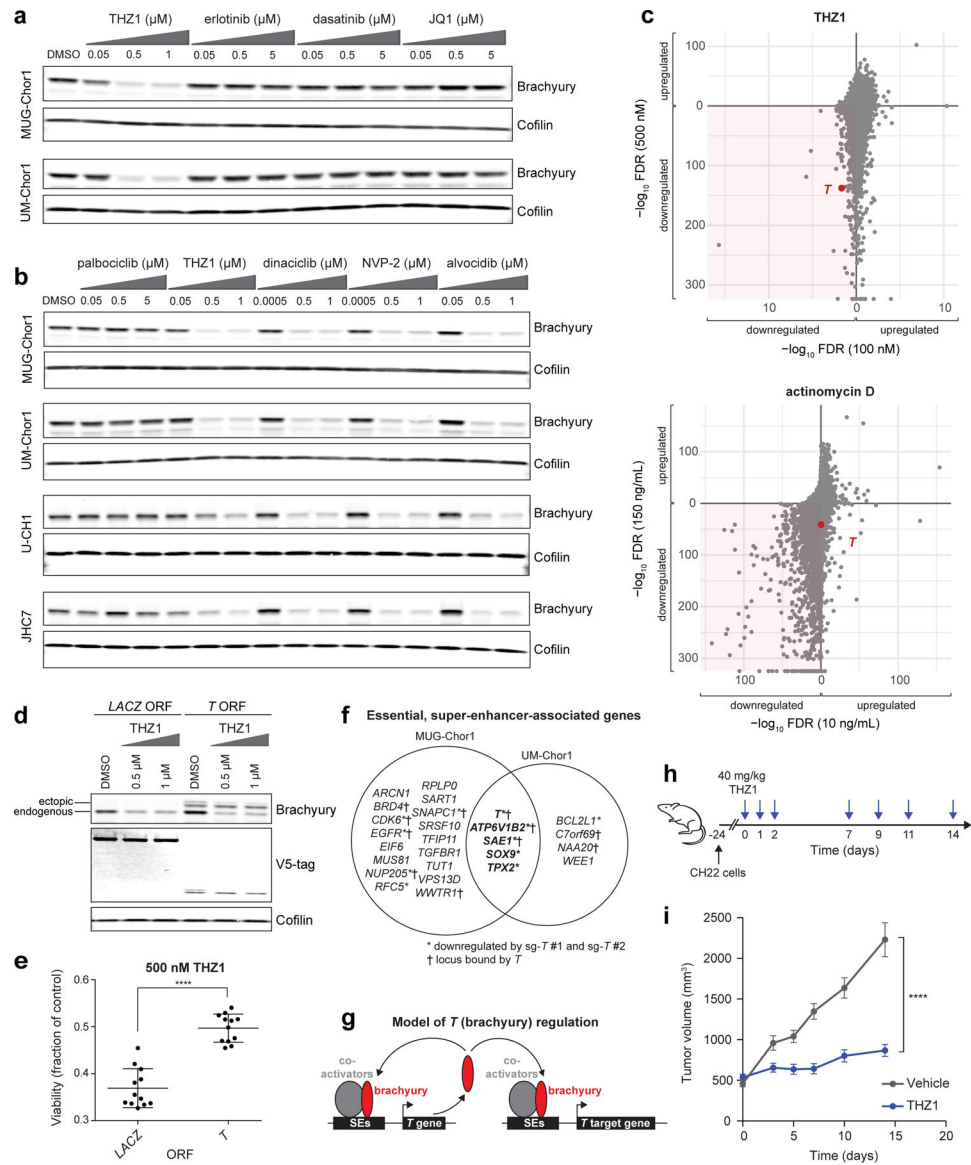
Figure 4. Inhibitors of CDK7/12/13 and CDK9 downregulate *T* (brachyury) expression, and THZ1 treatment reduces chordoma tumor proliferation *in vivo*.

a) Immunoblot analysis of chordoma cells treated with indicated concentrations of antiproliferative compounds or DMSO for 48 h. The experiment was performed four times with UM-Chor1 cells (one representative experiment displayed) and once with MUG-Chor1 cells. **b)** Immunoblot analysis of chordoma cells treated with indicated concentrations of inhibitors targeting CDK4/6 (palbociclib), CDK7/12/13 (THZ1), or CDK9 (dinaciclib, NVP-2, alvocidib) or DMSO for 48 h. The experiment was performed twice with MUG-Chor1, UM-Chor1, and U-CH1 cells (one representative experiment displayed for each) and once for JHC7 cells. **c)** Relative gene expression of UM-Chor1 cells treated with THZ1 (100 nM or 500 nM) (top), or actinomycin D (10 ng/mL or 150 ng/mL) (bottom), versus vehicle-treated cells. Cells were treated with compound or vehicle (DMSO) for 4 h. Gene-expression profiling was performed with RNA-seq, and genes downregulated following treatment with both concentrations of a given compound are indicated (shaded region). Ranked by

significance, *T* has a rank of 128 and 139 out of 37,043 genes for 100 nM and 500 nM THZ1, respectively; and a rank of 11,607 and 2,539 out of 37,043 genes for 10 ng/mL and 150 ng/mL actinomycin D, respectively. Data represent two biological replicates per condition, and false-discovery-rate (FDR) values were derived from a two-sided Wald test, with a Benjamini-Hochberg correction. **d)** Immunoblot analysis of UM-Chor1 cells transduced with V5-tagged ORFs encoding *T* or a *LACZ* control gene and then treated with indicated concentrations of THZ1. Unlike endogenous brachyury expression, ectopic brachyury expression was not greatly reduced with THZ1 treatment. The experiment was performed twice (one representative experiment displayed). **e)** Cell viability of UM-Chor1 cells transduced with an ORF encoding either *LACZ* or *T* and then treated with 500 nM THZ1. Data are expressed as the fraction of cell viability relative to vehicle-treated cells and represent the mean ± SD (n = 12 biological samples measured in parallel). **** p < 0.0001, derived from a two-tailed, unpaired t test. Exact p-values and effect sizes are reported in Supplementary Table 9. **f)** Integration of super-enhancer-associated and essential genes in UM-Chor1 and MUG-Chor1 cell lines. Essential genes were identified for each cell line by applying the STARS algorithm (see Methods) to genome-scale CRISPR-Cas9 screening data described in Fig. 1. Asterisk, genes downregulated following sg-*T*-mediated *T* repression as measured by RNA-seq (experiment described in Fig. 1d). Cross, gene loci bound by brachyury as measured by brachyury ChIP-seq (using a previously reported dataset[33]; see Methods). **g)** Model of *T* (brachyury) gene control. **h)** Schematic of the dosing schedule for THZ1 treatment of a human xenograft mouse model of chordoma. **i)** Tumor proliferation in mice engrafted with CH22 cells and treated with vehicle or THZ1. Data represent the mean tumor volume ± SEM of 12 (vehicle-treated) or 14 (THZ1-treated) mouse tumors at the indicated time points. **** p < 0.0001, derived from a two-way ANOVA with repeated measures. Exact p-values and effect sizes are reported in Supplementary Table 9.